Diversity of fate outcomes in cell pairs under lateral inhibition

Nara Guisoni[1,2,*], Rosa Martinez-Corral[1,*], Jordi Garcia Ojalvo[1,#], and Joaquín de Navascués[3,#]

[1] Department of Experimental and Health Sciences, Universitat Pompeu Fabra, Barcelona Biomedical Research Park (PRBB), Dr. Aiguader 88, 08003 Barcelona, Spain.

[2] Instituto de Física de Líquidos y Sistemas Biológicos, CONICET & Universidad Nacional de La Plata, Calle 59-789, 1900 La Plata, Argentina.

[3] European Cancer Stem Cell Research Institute, School of Biosciences, Cardiff University, Hadyn Ellis Building, Maindy Road, Cardiff CF24 4HQ, UK.

[*] Equal contribution

[#] Correspondence: denavascuesj@cardiff.ac.uk, jordi.g.ojalvo@upf.edu

Key words: Lateral inhibition, Notch-Delta signalling, symmetric cell division, intestinal stem cells, neutral competition

Summary statement: Notch/Delta-mediated lateral inhibition in cell pairs can result in symmetric signalling depending on the activation threshold, which can modulate cell-fate decisions depending on contact area.

Abstract

Cell fate determination by lateral inhibition via Notch/Delta signalling has been extensively studied. Most formalised models consider Notch/Delta interactions in fields of cells, with parameters that typically lead to symmetry breaking of signalling states between neighbouring cells, commonly resulting in salt-and-pepper fate patterns. Here we consider the case of signalling between isolated cell pairs, and find that the bifurcation properties of a standard mathematical model of lateral inhibition can lead to stable symmetric signalling states. We apply this model to the adult intestinal stem cell (ISC) of *Drosophila*, whose fate is stochastic but dependent on the Notch/Delta pathway. We observe a correlation between signalling state in cell pairs and their contact area. We interpret this behaviour in terms of the properties of our model in the presence of population variability in contact areas, which affects the effective signalling threshold of individual cells. Our results suggest that the dynamics of Notch/Delta signalling can contribute to explain stochasticity in stem cell fate decisions, and that the standard model for lateral inhibition can account for a wider range of developmental outcomes than previously considered.

Introduction

The Notch/Delta signalling pathway is one of the main regulators of cellular differentiation during development and adult tissue maintenance (reviewed in Artavanis-Tsakonas et al., 1999; Ehebauer et al., 2006; Koch et al., 2013). It often drives mutually inhibitory interactions between cells, acting as a gate for differentiation. This mode of action has been termed lateral inhibition, and has been the object of experimental study as well as mathematical formalisation for decades (see, for instance, Othmer and Scriven, 1971; Collier et al., 1996; Sprinzak et al., 2011; Petrovic et al., 2014). Quantitative models of lateral inhibition usually involve a field of cells expressing initially similar amounts of the receptor Notch and its membrane-bound ligand Delta. Delta trans-activates Notch in neighbouring cells and Notch, once activated, reduces in turn the ability of the cell to signal through Delta, leading to a state of mutual repression. This symmetry (and cell fate equivalence) is eventually broken by enforced biases and/or stochastic variation in Notch/Delta levels (Collier et al., 1996; Plahte, 2001; reviewed in Simpson, 2001) resulting in extended fine-grained spacing patterns (Othmer and Scriven, 1971; Collier et al., 1996; see also Shaya and Sprinzak, 2011) that have been experimentally characterized in depth in real developmental systems (reviewed in Greenwald, 1998; Arias and Stewart, 2002). In contrast, little attention has been paid so far to the effect of lateral inhibition in isolated cell pairs, beyond the trivial expectation that symmetry breaking will eventually take place, leading to cells taking opposing fates (see for instance, Collier et al., 1996; Rouault and Hakim, 2012). However there has been no formal investigation of whether alternative steady states are possible, perhaps due to the lack of an experimental model to relate it to.

The cellular homeostasis of the adult *Drosophila* midgut (Fig. 1A-D) can provide this experimental scenario, as in this tissue Notch/Delta signalling occurs mostly in isolated pairs of cells (Ohlstein and Spradling, 2006; de Navascués et al., 2012; Goulas et al., 2012). The fly's intestinal lining is maintained by intestinal stem cells (ISCs), which divide to both self-renew and

provide committed progenitors (Fig. 1B). Progenitors specialise in producing either nutrient-absorbing enterocytes or secretory enteroendocrine cells (Guo and Ohlstein, 2015; Micchelli and Perrimon, 2006; Ohlstein and Spradling, 2006; Zeng and Hou, 2015). The precursors of enterocytes, called enteroblasts (EBs) are frequently found forming pairs with ISCs (Ohlstein and Spradling, 2006; Micchelli and Perrimon, 2006; Bardin et al., 2010; de Navascués et al., 2012) (Fig. 1C). These pairs are thought to result from an earlier division of an ISC and subsequent fate allocation by Notch signalling, before a new division or terminal differentiation event takes place (Goulas et al., 2012; de Navascués et al., 2012). Importantly, ISC divisions in the enterocyte lineage result in either asymmetric fate (one ISC and an EB), or symmetric self-renewal (two ISCs) or differentiation (two EBs), which globally result in balanced, homeostatic proportions (de Navascués et al., 2012) (Fig. 1D). This mode of tissue maintenance, whereby the balance between stem cell self-renewal and differentiation is achieved at the population level rather than within every stem cell lineage, is termed neutral competition (Klein and Simons, 2011) and is found in a growing number of self-renewing adult tissues (Simons and Clevers, 2011). While no molecular mechanism has been fully elucidated so far for any case of neutral competition, in the fly gut it has been proposed to arise from lateral inhibition mediated by Notch/Delta (de Navascués et al., 2012), a pathway known to define the fate of the ISC offspring (Ohlstein and Spradling, 2006; Micchelli and Perrimon, 2006; Bardin et al., 2010).

Here we explore the capacity of a standard model of lateral inhibition acting in pairs of interacting cells to result in steady states with different signalling states (either symmetric or asymmetric) coexisting in the tissue. We find that this is indeed possible, provided signalling thresholds vary across cell pairs. Next, we turn to the *Drosophila* midgut and find that the tissue displays high variability of contact area between pairs of ISC/EB cells, which can be associated to an effective heterogeneity in signalling thresholds between pairs of cells. When contrasting this variability with the distribution of fate combinations in pairs of ISC/EB cells, we find a correlation between contact

area of specific cell pairs and their fate profile. Moreover, our model can reproduce the distribution of fate outcomes given the contact area distribution determined experimentally.

Our results expand the repertoire of possible outputs of a system governed by lateral inhibition, and connect this mode of signalling with a mode of stem-cell based tissue maintenance (neutral competition) that is highly relevant in adult tissue homeostasis and tumourigenesis (Simons and Clevers, 2011; Vermeulen et al., 2013; Baker et al., 2014), and whose molecular regulation is poorly understood.

Materials and Methods

The model: lateral inhibition mediated by Notch-Delta interaction

We consider that the rate of Notch activation in a cell is an increasing function of Delta concentration on its neighbour (signalling), and that the rate of Delta expression is a decreasing function of the level of activated Notch in the same cell (inhibition). We represent these interactions by means of a standard mathematical model of Notch/Delta signalling (Collier et al., 1996) between pairs of cells, which is given by:

$$\frac{d\overline{N}_1}{dt} = \alpha f(\overline{D}_2) - \delta_N \overline{N}_1, \quad (1)$$

$$\frac{d\overline{D}_1}{dt} = \beta g(\overline{N}_1) - \delta_D \overline{D}_1, \quad (2)$$

$$\frac{d\overline{N}_2}{dt} = \alpha f(\overline{D}_1) - \delta_N \overline{N}_2, \quad (3)$$

$$\frac{d\overline{D}_2}{dt} = \beta g(\overline{N}_2) - \delta_D \overline{D}_2. \quad (4)$$

Here $\overline{N}_{1,2}$ represent the levels of Notch activity in cells 1 and 2, and $\overline{D}_{1,2}$ are the concentrations of Delta in each cell. α and β are the maximal production rates of Notch and Delta, respectively, whereas δ_N and δ_D are their corresponding degradation rates. The production terms for Notch (f) and Delta (g) are given by the Hill functions

$$f(\bar{D}) = \frac{\bar{D}^r}{K_N^r + \bar{D}^r}, \qquad g(\bar{N}) = \frac{1}{1+(\bar{N}/K_D)^h}, \tag{5}$$

where the first function represents the signalling effect of Delta on the neighbouring cell, and the second corresponds to the inhibition of Delta expression by activated Notch in the same cell. K_N is the threshold of Notch activation by neighbouring Delta, K_D is the threshold of Delta inhibition by Notch in the same cell, and the coefficients r and h represent the cooperative character of the two aforementioned processes. Similarly to (Collier et al., 1996) we rewrite Eqns 1- 4 in dimensionless form as:

$$\frac{dN_{1,2}}{dt} = \frac{D_{2,1}^r}{a^r + D_{2,1}^r} - N_{1,2}, \qquad \frac{dD_{1,2}}{dt} = \nu\left(\frac{1}{1+\left(\frac{N_{1,2}}{b}\right)^h} - D_{1,2}\right) \tag{6}$$

The parameter ν is the ratio between the degradation rates of Delta and Notch, δ_D/δ_N. a and b are the dimensionless thresholds for Notch activation by Delta in the neighbouring cell, and Delta inhibition by Notch in the same cell, respectively,

$$a \equiv \frac{K_N \delta_D}{\beta} \equiv \frac{c}{A}, \qquad b \equiv \frac{K_D \delta_N}{\alpha}. \tag{7}$$

a and b are referred to as the activation and inhibition thresholds, and their values set the location of the half-maximal points of the Hill functions in Eqn 6. Importantly, the signalling threshold a is considered to depend explicitly on the contact area A between the two interacting cells, since a larger contact area will effectively reduce the threshold of Notch activation, by increasing the number of receptors available to bind ligands from the sending cell. The constant c is treated as a parameter of the model.

We studied the behaviour of the system on a region of the a-b parameter space that spans a biologically plausible range, according to data from the literature for K_N (Sprinzak et al., 2010; Pei and Baker, 2008), K_D (Friedmann and Kovall, 2010), α, β (Agrawal et al., 2009), δ_N (Hsu et al., 2006; Agrawal et

al., 2009), and δ_D (Hsu et al., 2006). For fixed Hill coefficients r and h, the parameters a and b determine the steady state of the system.

Steady states and cell fate identification

The system of equations (6) has a homogeneous steady state in which Notch and Delta have the same values in the two cells:

$$N^* = f(D^*), \qquad \mathrm{D}^* = g(N^*)$$

This state corresponds to a situation in which both cells in the pair have the same fate. The stability boundary of this homogeneous steady state can be calculated using standard methods (Collier et al., 1996), and is represented by a dotted line in Fig. 2A. Above this line the homogeneous state is stable. Below it, a heterogeneous stable steady state appears in which the values of Notch and Delta are different between the two cells:

$$N_1^* = f(D_2^*), \qquad D_1^* = g(N_1^*),$$

$$N_2^* = f(D_1^*), \qquad D_2^* = g(N_2^*).$$

In parallel with this classification of steady states, a cell is considered to be Notch positive when the level of Notch surpasses a certain threshold N_{thr} (considered here to be 0.1), and Notch negative in the opposite case. In the case of the *Drosophila* midgut, a Notch positive cell would correspond to an EB, and a Notch negative cell to an ISC. In that way, a homogeneous steady state can represent either an ISC/ISC pair (symmetric Notch negative, blue region in Fig. 2A) or an EB/EB pair (symmetric Notch positive, green region in Fig. 2A). Most heterogeneous steady states, in turn, correspond to an ISC/EB pair (orange region in Fig. 2A), although heterogeneous states in which both values of Notch lie below (or above) the threshold N_{thr} still represent symmetric ISC/ISC (or EB/EB) pairs. This is reflected in Fig. 2A through the difference between the stability boundary (dotted grey line) and the boundaries between the fate-pair domains shown in colour code.

Dynamical behaviour

We investigate the temporal evolution of the model by solving numerically the Equations (6). For this purpose, we use a finite difference approximation (two-stage Runge-Kutta; LeVeque, 2007). In our calculations, we are considering $r = h = 2$ and $\delta_N = \delta_D$, as in previous works (Collier et al., 1996; Sprinzak et al., 2010). Cells are considered initially negative for Notch activation (Ohlstein and Spradling, 2007; Guo and Ohlstein, 2015).

Drosophila culture and strains

Adult flies were raised in standard cornmeal medium, collected daily and maintained in fresh vials with added yeast (food replaced every 24-48h). Untreated flies were dissected at 4-6 days of age. Mifepristone (RU486) treated flies were treated as described above and transferred to RU486-containing medium at 3-8 days of age for three more days before dissection.

EBs were identified by co-expression of one of two enhancer trap reporters of the undifferentiated cell marker *escargot* (FlyBase: *P{PTT-GB}esg*^{YB0232}; Quiñones-Coello et al., 2007; or *P{lacW}esg*^{k00606}; Spradling et al., 1999) and one of two *GBE-Su(H)* synthetic reporters of Notch transcriptional activity (Bray and Furriols, 2001; de Navascués et al., 2012) while ISCs were identified by expression of the *esg* reporter alone (Micchelli and Perrimon, 2006; Ohlstein and Spradling, 2006).

Delta levels were measured with the *Delta*$^{MI04868\text{-}GFSTF.1}$ transgenic insertion (FlyBase *Mi{PT-GFSTF.1}Dl*$^{MI04868\text{-}GFSTF.1}$), which tags all three annotated Delta isoforms with GFP at the endogenous locus (Nagarkar-Jaiswal et al., 2015).

Genetic perturbation of Notch activity was performed (1) by knockdown with *da-GS* (FlyBase: *P{da-GSGAL4.T}*; Tricoire et al., 2009) and *UAS-Notch*^{RNAi} (FlyBase: *P{w[+mC]=UAS-N.dsRNA.P}14E*; Presente et al., 2002), activated with mifepristone (RU486, Sigma), with mock treatment as control, or (2) by using the molecular null allele *N*^{55e11} (Kidd et al., 1983) or the Delta-dependent, hypermorphic *l(1)N*^{B} (FlyBase: *N*$^{l1N\text{-}B}$; Lyman and Young, 1993; Brennan et al., 1997), with *Oregon R* as wild-type control.

Immunohistofluorescence and imaging

Immunofluorescence was performed essentially as described in (Bardin et al., 2010) but with a heat fixation step (Miller et al., 1989). This fixation method was essential for the robust immunodetection of Armadillo (Fang et al., 2016).

Primary antibodies were: chicken anti-β-Galactosidase (Abcam ab9361, 1:200), rabbit anti-GFP (Abcam ab6556, 1:200), sheep anti-Notch (Muñoz-Descalzo et al., 2011; 1:1000), anti-Arm (mAb N2-7A1, 1:50) and anti-Dl (mAb C594.9B, 1:50). The N2-7A1 and C594.9B antibodies were obtained from the Developmental Studies Hybridoma Bank (NICHD and The University of Iowa). Secondary antibodies conjugated with Alexa fluorophores were from Invitrogen (1:500). Of note, immunodetection of *GBE-Su(H)-lacZ* expression in heat-fixed material was less sensitive than that of *GBE-Su(H)-GFP:nls*; this might have led to an underestimation of EBs numbers, which in any case will have played against our hypotheses.

Confocal stacks were obtained in a Zeiss LSM 710 with an EC Plan-Neofluar 40X oil immersion objective (numerical aperture 1.3). For the quantification of membrane features, voxel sizes were 0.22x0.22x0.6, 0.21x0.21x1, or 0.18x0.18x0.6 (contact area), 0.16x0.16x0.7 μm (distribution of Notch and Armadillo), or 0.14x0.14x1 μm (distribution of Delta), with airy units adjusted so that there was negligible oversampling in Z, or not at all.

Image analysis

To measure contact area, stacks were analysed with a combination of ImageJ macros and python scripts to (1) manually identify all esg-GFP$^+$ cells in a z-projection of the stack, (2) automatically threshold *GBE-Su(H)-lacZ* reporter expression in 3D to determine its expression status (positive or negative) in every esg$^+$ cell, followed by a step of manual correction, (3) manually identify the nests of esg$^+$ cells so that (4) a series of 3D stacks, containing only one pair each, is automatically cropped, and (5) the contact membrane of each esg$^+$ cell pair is semi-automatically determined using FIJI for each optical plane, by binarising the immunofluorescence of Armadillo/*β*-catenin (Arm).

Arm labels the membrane throughout the apical-basal axis (see Results), which allows measuring the amount of contacting membrane in each cell pair as the number of Arm^+ voxels shared between the two cells (expressed in μm^2).

To measure cell size, the cellular perimeter in 3D was used to measure the volume enclosed. Alternatively, we projected the maximum intensity of Arm in the Z dimension and calculated the area enclosed in the projected perimeter of the cell as the 'projected area'. This measurement correlated well with the cell volume (Fig. S6A).

To evaluate the co-localisation between Delta:GFP and anti-Delta, $Delta^+$ cells appriopriately immunostained were manually identified and individually outlined in 2D in several fields of view (comprising a few hundred enteric cells each). For each outline, the enclosing 3D stack was automatically extracted, and the Pearson correlation and the Manders co-localisation (Manders et al., 1993) coefficients were calculated between different pairs of channels.

For measuring Notch, Delta and Arm distribution at the membrane, the membrane contours (3-4 pixels wide) of cells in pairs were manually determined in each plane. At the spatial resolution of our micrographs, it is not possible to distinguish, for a pixel at the boundary, to which cell of the pair it belongs, so we took the approximation of splitting the thickness of the contact between the two cells. Intensity data from those positions were used as described in what follows.

Intensity normalisation. For each plane in the confocal stack, an empty 50x50 pixel square nearby each of the cell pairs in that stack was manually selected. The signal therein (for all the planes in the stack where membrane was detectable) was averaged for all the squares of the same stack, and this value was taken as background. Notch, Delta and Arm intensity values for each stack were normalised by dividing by the background value.

Distribution along cell perimeter. In each confocal plane, each membrane pixel position was assigned an angular value respect to the centroid by

calculating its tangent arc (±π depending on the quadrant). Thirty overlapping sliding windows (of 2π/15 rad with half window overlap) were delimited in each plane, and their pixel intensities were normalised and averaged.

Distribution along the apical-basal axis. Each cell was sliced in 10 overlapping angular windows (2π/5 rad with half overlap). For each window, a normalised, average intensity measurement was taken per confocal plane (i.e. along the apical-basal axis). Apical-basal positions were normalised from 0 to 1. Intensity data points along the apical-basal axis were obtained by interpolation from average normalized intensity values.

Results

Lateral inhibition can result in stable, opposing symmetric signalling states

We study the steady-state behaviour of a standard model of lateral inhibition for the case of two cells (see Methods). For fixed r and h, the steady states of this system depend on two parameters, a and b (the dimensionless activation and inhibition thresholds, respectively; see Methods), which we allow to vary across the population of cell pairs. We then calculate the equilibrium state of the system in this two-dimensional parameter space, according to the resulting signalling profile: asymmetric (one cell positive for Notch activation and the other one negative, see Methods), symmetric positive, or symmetric negative for Notch activation (Fig. 1C). Thus, for a population of cell pairs with variable activation or inhibition thresholds (a and b), the three possible signalling state profiles occur (Fig. 2A, see Fig. 2B-E for a comparison of the dynamic evolution of examples of the three profiles, with Fig. 2B corresponding to the parameter values from Collier et al., 1996). The three signalling state profiles can be found within a relatively short range of parameter values (Fig. 2A). Importantly, this scenario does not change qualitatively when considering a wide range of threshold values for Notch activity classification, as defined in the Methods section ($0.001 \leq N_{thr} \leq 0.8$; Fig. S1B-E), or higher cooperativity values in Notch signalling or Delta inhibition ($r, h = (2,5)\ or\ (5,2)$) (Fig. S1F-G). However, we found that

cooperativity was necessary: for $r = 1$, $h = 1$, the heterogeneous (asymmetric) steady states are lost (Fig. S1H). This requirement of cooperativity is in agreement with other theoretical works on lateral inhibition (Sprinzak et al., 2011) as well as with *in vitro* estimates for r of 1.7 (Sprinzak et al., 2010).

In a biological system, the existence of three possible signalling state profiles would be equivalent to having three different cell fate combinations across a population of initially uncommitted cell pairs interacting through Notch/Delta, with the specific fate combination of a given cell pair depending on the sensitivity to Delta activation and Notch inhibition of the pair. To investigate the potential of this lateral inhibition model, incorporating variable activation and inhibition thresholds, to describe a real biological system, we turned to the *Drosophila* midgut.

Cell pair type frequencies correlate with Notch activity

As mentioned in the Methods section, in the *Drosophila* midgut Notch negative cells correspond to ISCs, and Notch positive cells to EBs. The Notch activity reporter *GBE-Su(H)* is hardly expressed above background levels in ISCs (Ohlstein and Spradling, 2007; and our own observations), and hence our choice of a low threshold value, $N_{thr} = 0.1$. Symmetric positive pairs in the model will equate to an event of symmetric differentiation (EB/EB), symmetric negative pairs to symmetric self-renewal (ISC/ISC), and asymmetric pairs to asymmetric ISC fate (ISC/EB) (Fig. 2A). If this was the case, we would expect the relative frequencies of these pairs to correlate with overall *Notch* activity levels, as has been shown with the balance of the whole population of ISC and EB levels (Biteau et al., 2008; de Navascués et al., 2012). Indeed, heterozygous conditions for the null allele N^{55e11} lead to more ISC-ISC pairs and less EB-EB pairs relative to the wild-type, whereas heterozygosis for the hyperactive, Dl-dependent $l(1)N^{B}$ mutation favours EB-EB pairs at the expense of ISC-ISC pairs, whose presence is negligible (Fig. 1E). To ensure that these differences are due to variations in Notch activity, rather than to the genetic background of the different mutant chromosomes, we did a serial

knock-down of *Notch* in ISCs and EBs. To that end, we used the GeneSwitch system (Osterwalder et al., 2001) with the driver *da-GS*, which is largely specific of ISCs and EBs in the intestine (Fig. S2A and Nicolas Buchon, personal communication), and increasing concentrations of the inducer RU486. In these experiments, the flies share the same genetic background, and only differ in the amount of RU486 present in the food. Indeed, we find that mild knock-down of *Notch* (to a level that does not yet lead to ISC-like tumour growth; Fig. S2B-F), increases the number of ISC-ISC pairs at the cost of ISC-EB and EB-EB pairs, in a dose-dependent manner (Fig. 1F). Note that the baseline fractions of the control for the induction experiment ('mock' bars in Fig. 1F) are different from the control for the mutants ('$N^{+/+}$' bars in Fig. 1E), even if at the overall level the total numbers of ISCs and EBs are balanced (Fig. 1G, H; de Navascués et al., 2012), highlighting the importance of controlling for genetic background in these experiments. From these data we conclude that the frequency of undifferentiated pair types are a good readout of the strength of Notch signalling.

Cell contact area as modulator of activation threshold

To relate the model to real tissue, we need first to consider how the dimensionless parameters a and b are related to biological features displaying variability across undifferentiated (esg$^+$) cell pairs. We assume that biochemical processes intrinsic to the cell, such as protein degradation rates (δ_D and δ_N), the maximal biosynthesis rates (α and β), and the threshold of Delta inhibition by Notch in the same cell (K_D), will not be highly variable among cells with a common developmental identity. On the other hand, the threshold of Notch activation by neighbouring Delta (K_N) depends directly on the interaction between the two cells, which could be variable for different pairs of cells. For instance, due to spatial heterogeneity of cell packing, the contact area between cell pairs could be substantially different from pair to pair. Indeed, tissue images reveal that undifferentiated cells in nests show irregular shapes and variable contact area (Fig. 3A). In the Notch/Delta system the amounts of Notch and Delta are usually limiting, and this seems to

hold true for the adult *Drosophila* gut, where haploinsufficiency has been described (Biteau et al., 2008; de Navascués et al., 2012; see also Fig. 1E-H). Therefore, it is expected that variations of ~2-fold or more in contact area would lead to significant changes in the levels of Notch activation. This is captured in the model by expressing the dimensionless activation threshold a in terms of the contact area, following Eqn 7 above. Specifically, we assume that a is inversely related with the contact area (the larger the contact area, the easier it is for Delta to activate Notch, and thus the smaller the activation threshold). As shown in Fig. 2A (see also Fig. S3), variation in a best allows for heterogeneity in stable steady state levels of Notch activity and therefore in fate choice. From this we hypothesize that variation of contact area (or any other biological feature correlating with the threshold of Notch activation) is likely to allow the diversity in fate outcome predicted by the model.

The above-mentioned assumption by which the activation threshold depends inversely on the contact area requires Notch and Delta proteins to be homogeneously distributed across the cell surface (such that their probability of binding increases with the area of contact). To evaluate this, we used confocal microscopy to examine the localisation of both Notch and Delta proteins respect to the membrane marker Armadillo/*β*-catenin (Arm), in both single and paired ISCs and EBs in the midgut epithelium (Fig. 3B-C). In *Drosophila* epithelia, Arm/ β-cat participates in the formation of adherens junctions, which localise mostly in the apical domain, with lower levels at the lateral membrane (Tepass and Hartenstein, 1994). Therefore, we used Arm staining to define membrane boundaries in 3D, and measured the intensity of Arm, Notch, and Delta:GFP proteins at the cell membrane. The latter is an endogenously tagged protein which correctly represents the localisation of the wild-type Delta both visually and by co-localisation analysis (Fig. S4; see also Nagarkar-Jaiswal et al., 2015).

We could not find any strong pattern in the variations of Notch or Delta immunodetection intensity within confocal planes, and it would only seem that both are slightly enriched at the boundary between two undifferentiated cells

(Fig. 3E-F). This indicates that Notch and Delta concentrations are largely independent of the position at the membrane along the cell perimeter, and in particular along the contact between esg^+ cells. Moreover, the localisation of both Notch and Delta along the apical-basal axis of the cells is also largely homogeneous (Fig S5E,F). This is manifest in the small variation in the average amounts of Notch and Delta between different optical planes (Fig. S5B-C, left panels), and in the narrow distribution of mean values per plane, with low values of coefficients of variation per plane, of Notch intensity values (Fig. S5B-C, right panels). Therefore, the contact area between cells is a good approximation to the total amount of Notch and Delta proteins available for signalling.

We note that Arm largely parallels Notch and Delta localisation at the membrane (Figs. 3D and S5D) but shows a stronger enrichment at the boundary (Fig. 3D), in agreement with previous reports (Maeda et al., 2008). Incidentally, these results also reveal that neither Arm nor Notch nor Delta are restricted to the apical domain in the midgut epithelium**,** and instead can be found in similar amounts along the apical-basal axis of the membrane in ISCs and EBs (Fig. S5D-F). This situation contrasts with Arm and Notch distribution in other Drosophila epithelia (Tepass and Hartenstein, 1994; Tepass et al., 2001; Sanders et al., 2009).

Taken together, our results suggest that both the Notch receptor and its ligand Delta are randomly and homogeneously distributed in the cell membrane, which suggests that measurements of membrane contact area may be relevant to the dynamics of Delta-Notch signalling as a proxy for the activation threshold a in our model.

Correlation of contact area values and cell fate profiles

We have shown that contact area can be used as a measure of the amount of Notch and Delta available for interaction. Therefore, our model predicts that contact area should correlate with the patterns of symmetric and asymmetric fates. Indeed, we observe increasing average contact area in ISC-ISC ($7.67\mu m^2$), ISC-EB ($13.28\mu m^2$) and EB-EB ($14.79\mu m^2$) cells (Fig. 4A). The

contact area in ISC-ISC pairs was significantly lower than in the other two cell-pair types (with *p*-values of 0.002 and 0.005 when compared with ISC-EB and EB-EB pairs, respectively), while the latter could not be statistically distinguished from each other ($p = 0.5$). We must also remark that EB cells increase in size after they progress from their original ISC state (Fig. 4B and S6B), which complicates our interpretation of the correlation between fate and contact area, especially in EB-EB pairs. This fact, together with the statistical similarity between ISC-EB and EB-EB pairs mentioned above, led us to focus on the distinction between ISC-ISC and ISC-EB, filtering the results coming from the latter cell-pair type based on the size of the EB cells (see below).

We measured the contact areas in 480 pairs of esg^+ cells with both symmetric (ISC-ISC, n=74) and asymmetric (ISC-EB, n=406) fates. The data show that contact area in these pairs is highly variable, ranging from just around $1\mu m^2$ to over $40\mu m^2$ (Fig. 4C). This degree of variability (of more than one order of magnitude) indicates that contact area has the potential to be a regulatory mechanism of the system (through its influence on the dimensionless activation threshold a).

Next, we classified measurements of contact area according to the fate profile of their corresponding cell pair and compared their values (Fig. 4D). We found that the cumulative distributions of contact areas in ISC-ISC and ISC-EB pairs are clearly separated. On average, the contact area between two ISCs (11.59 ± 0.73 μm^2; mean ± standard error of the mean) is clearly smaller than that between an ISC and an EB (17.68 ± 0.42 μm^2) ($p = 8\times10^{-7}$). To verify that this correlation is not simply a consequence of EBs being larger, we compared the distributions of contact areas between ISC-ISC pairs and different subsets of ISC-EB pairs which included only the pairs where the EB member was smaller than a given size limit (1x, 0.75x and 0.5x the maximum ISC size, respectively). The effect of the thresholding on the distribution of cell sizes (measured in terms of the projected areas) is shown in Fig. 4E. Note that as the threshold decreases the average size of the filtered EBs is progressively smaller, until it can no longer be statistically discriminated from the distribution

of ISC sizes (for the subset with size limit equal to half the maximum ISC size, $p = 0.07$). However, the corresponding contact area distributions of these subsets of ISC-EB pairs are all strikingly similar, with values systematically larger than those of ISC-ISC pairs at a high level of significance (maximum p-value = 2×10^{-4}) (Fig. 4F). This is in good agreement with the fact that the cell size of the pair members and their contact area are not correlated (Fig. S6C-D).

We also wanted to check that the differences in cell-pair types discussed above are not associated with differences in adhesion properties between ISCs and EBs, as could be suggested by the fact that Arm levels are enriched at the contact area between these cell pairs (Fig. 3D). For this, we measured the values of Arm at the boundary of ISC-ISC pairs and ISC-EB pairs. Since we cannot distinguish which cell of the pair originates the Arm signal at the boundary (see Materials and Methods), we measured the signal assigned to ISCs in either ISC-ISC pairs or ISC-EB pairs, as an approximation to the strength of adhesion at the boundary of these cell pairs. We found a similar, moderate increment in Arm levels at the cell pair boundary in both ISC-ISC and ISC-EB pairs (Fig. S6E-F), indicating that adhesion properties are not fundamentally different between cell pair types (at least as far as adherens junctions are concerned). This fits well with the observation that the transcriptional profiles of ISCs and EBs are not particularly enriched in genes involved in cell adhesion (Dutta et al., 2015).

Taken together, these results indicate that a smaller contact area correlates with the ISC-ISC pair profile, and this is likely linked to a higher activation threshold of Notch in ISC-ISC pairs, rather than to changes in cell shape, size or adhesion properties in the ISC-EB pairs posterior to EB fate acquisition.

Updating the model with area variation reproduces fate profile distributions

This finding gives us biological justification to consider the activation threshold a to be variable in the model (inversely proportional to the contact area), and test the capacity of the model to produce the observed proportions of fate

pairs in our various experimental conditions (Fig 1E, F). To do this, we first generated a large sample of contact area values *A*, from a Smooth Kernel Distribution based on the experimental data (Fig. 4C). To input values from *A* into the model, we simply used Eqn. 7 ($a \equiv c/A$). We then analysed the stable steady states of the model, obtaining the proportions of the three possible fate pairs resulting from *A*, for different values of b and c.

In order to compare the fate distribution obtained from the model and the experimental datasets we use the Kullback-Leibler relative entropy (*H*), which is a dissimilarity measure between two probability distributions (giving the value 0 if the distributions are equal; Kullback and Leibler, 1951). We found an excellent agreement between the proportions of EB-EB, EB-ISC and ISC-ISC pairs observed experimentally, and the distributions from the model for an extended range of values of b and c, as indicated by the low values of *H* between theoretical and experimental distributions (see Fig. S6G-H). Ranges of values for parameters a and b with good fit for each experimental condition are mapped to the model phase diagram in Fig. 4G (upper panel for *Notch* mutant and wild-type alleles; lower panel for RU486-induced *Notch* knock-down and the mock treatment), with corresponding pair frequencies (data and model) and parameter values (c, average b) given in Table 1 (with *H* values ranging from 1.8×10^{-4} to 1.6×10^{-2}). Focusing on the control datasets (*Notch* wild-type and *Notch* mock knock-down, Fig. 4G) one finds that ISC-ISC pairs occur at the lowest values of contact area (largest values of a), in good agreement with our experimental observations (Fig. 4A, D, F). In this region of parameter space, EB-EB and ISC-EB pairs are found at higher values of contact area (lower a), although we cannot distinguish statistically between the experimentally measured contact areas of these two cell-pair types (Fig. 4A). Importantly, we find that the regions of the parameter space where the model fits each of the mutant and knockdown experimental distributions correspond to parameter changes in line with the nature of the genetic perturbations. First, for all loss-of-function conditions of *Notch* (*Notch* knockdown and $N^{55e11/+}$ heterozygotes), the model can account for the

observed pair frequencies with small shifts in the b parameter and more substantial changes in the a parameter (note the very different scale ranges for a and b in Fig. 4G). The shifts towards higher a values can be explained as an increase in the K_N parameter (i.e. lower activation of Notch for a given Delta stimulus; see Eqns. 5 and 7), which fits the nature of a loss of function condition. In the case of *Notch* gain of function, represented by the $N^{l1N\text{-}B/+}$ hypermorphs, the model can reproduce the resulting pair frequencies by substantially reducing both a (therefore decreasing K_N, i.e. more Notch activation for the same Delta stimulus) and b (which can be accounted for as an increase of α, the maximal rate of Notch activation; see Eqn. 7); again, both notions sit well with the nature of the $l(1)N^{B}$ allele (a Delta-dependent, hypermorphic allele).

Our experimental observations thus agree with the model predictions, including both gain and loss of function perturbations of Notch signalling. Hence, our results confirm that the contact area between pairs of cells can influence the fate outcome of Notch/Delta signalling in the *Drosophila* midgut (Fig. 4H), with small contact area clearly favouring symmetric self-renewal.

Discussion

We have considered a standard model of Notch/Delta-mediated lateral inhibition (Collier et al., 1996) and investigated the effect of the trans-activation of Notch by Delta and the inhibition threshold of Delta by Notch signalling (here considered phenomenologically as the dimensionless thresholds a and b, respectively) on the dynamics of lateral inhibition for a system of two cells. We find that, provided there is a degree of variability in contact areas between cell pairs, three different signalling states (and therefore fate combinations) can occur under the same conditions. This is a considerable expansion of the model, whose use has so far been mostly centred on solutions that provide fine-grained (checkerboard) patterns. The model reproduces the signalling outcomes observed in the *Drosophila* intestine, which translate into differentiation vs. self-renewal fates. Thus, our results provide a mechanism whereby ISCs may undergo neutral competition,

549 which is a widespread pattern of adult tissue maintenance in metazoans from
550 *Drosophila* to humans.

551 The work by Collier et al. (1996) established a minimal model of lateral
552 inhibition as a system leading to checkerboard patterns of stable, all-or-none
553 signalling states. Their formalisation, and choice of parameters, has become a
554 reference in the field (Sprinzak et al., 2011; Formosa-Jordan et al., 2012;
555 Petrovic et al., 2014). However, to allow accommodating phenomenology that
556 departs from the classical fine-grained, all-or-none patterns, expansions of
557 this model have required the introduction of additional genetic components
558 (e.g. an extra ligand; Boareto et al., 2015) or noise components (de Back et
559 al., 2013). By contrast, here we have left intact the general dynamics of the
560 minimal model and simply introduced a degree of variability in the sensitivity
561 of each cell pair to signal transduction.

562 Our work considers the contact area between cells engaged in signalling as
563 the source of variation in signalling threshold. Contact area can be an
564 effective tuning parameter of a biological system (Khait et al., 2015), since it
565 can integrate mechanical constraints into signalling, as it has been shown for
566 cell density and proliferative control by the Hippo pathway (Schlegelmilch et
567 al., 2011; Kim et al., 2011; Silvis et al., 2011). In a system such as the
568 posterior midgut, where some differentiated cells are much larger than their
569 progenitors (see Fig. 1A), differentiated and mature cell loss certainly would
570 have a local impact in the packing geometry of cells interacting via
571 Notch/Delta, and connect naturally with the fate outcome of stem cell
572 divisions. This could be particularly useful in conditions of regeneration.
573 Importantly, our theoretical framework could in principle accommodate any
574 source of variation; for instance, variation arising from the unequal (either
575 random or regulated) inheritance of signalling components could result in
576 variation in the capability of signal transduction in the population. It is
577 interesting to consider that while shortly after division most of the ISC
578 daughter cells display similar levels of Notch and Delta proteins (Ohlstein and
579 Spradling, 2006), endosomes bearing the signalling molecule Sara display an

inhomogeneous inheritance pattern (Montagne and González-Gaitán, 2014). It has recently been found that ISC divisions producing enteroendocrine cell precursors do seem to segregate Delta asymmetrically towards the precursor cell (Guo and Ohlstein, 2015), which suggests that ISCs switch between different types of cell division.

Understanding how Notch/Delta signalling results in stochastic cell fate patterns is of particular relevance in adult homeostatic tissues, as Notch signalling controls fate in many types of tissue stem cells (Koch et al., 2013). Moreover, many adult stem cells balance their fate via neutral competition (Krieger and Simons, 2015). Our model proposes a mechanism whereby Notch/Delta signalling could result in neutral competition of stem cells by lateral inhibition between sibling cells. This provides an alternative explanation to the neutral competition of *Drosophila* adult ISCs, which has been proposed to arise from Notch/Delta-mediated lateral inhibition involving the offspring of non-related ISCs, coinciding in space (de Navascués et al., 2012) and resolving 20% of the time in symmetric fate. Although the two proposals are compatible with each other, the latter faces the difficulty that ISC/EB nests rarely contain more than two cells (de Navascués et al., 2012). Moreover, we and others have found isolated pairs of ISCs or EBs frequently in the tissue (de Navascués et al., 2012; Goulas et al., 2012). Our model provides a potential explanation of how the offspring of a single ISC (pairs of Notch/Delta signalling cells) may reach a symmetric steady state, leading to symmetric self-renewal or differentiation.

It would be interesting to see how our model translates to a larger group of interacting cells, in particular in light of recent findings in the oesophageal epithelium. There, tissue is maintained by the neutral competition of basal progenitor cells (Doupé et al., 2012), and this competition is heavily influenced by Notch signalling, to the point that alterations in the pathway can lead to the fixation of mutant clones and poise the tissue for tumour initiation (Alcolea et al., 2014).

Acknowledgements

We wish to acknowledge support from CONICET to NG and from Cardiff University to JdN. JGO and RMC are supported by the Spanish Ministerio de Economía y Competitividad and FEDER, through project FIS2015-66503-C3-1-P, and the ICREA Academia Programme. RMC also acknowledges financial support from La Caixa Foundation. We would like to thank Alfonso Martínez Arias for his encouragement and support and Nicole Gorfinkiel and David Sprinzak for critical comments on the manuscript.

Competing Interests

No competing interests declared.

Figure Legends

Figure 1. Tissue maintenance in the *Drosophila* adult midgut and effect of mild genetic perturbations of Notch signalling. Scale bars: 20μm. **A**. Confocal micrograph showing the cell types present in the midgut epithelium. ISCs are esg-GFP$^+$ (blue) and EBs are esg-GFP$^+$ and GBE-Su(H)-lacZ$^+$ (green). The two differentiated cells, enteroendocrine cells and enterocytes, are recognisable by Prospero (Pros) expression and having large, polyploid nuclei (Hoechst, grey), respectively. **B**. ISCs self-renew and produce EBs (which will terminally differentiate without further division). **C**. Confocal micrographs showing examples of cell pair type profiles: asymmetric (i), symmetric Notch negative (two ISCs, ii) and symmetric Notch positive (two EBs, iii). **D**. ISCs balance self-renewal and differentiation by dividing either asymmetrically (one ISC and an EB), or symmetrically into two ISCs or two EBs. **E**. Observed frequencies of the pair types depicted in C, D for wild type (n=235), hypermorphic (*l(1)N^B/+*, n=209) and hypomorphic (*N$^{55e11/+}$*, n=213) conditions for *Notch*. **F**. Observed frequencies of the pair types depicted in C, D for *da-GS, UAS-N^{RNAi}* flies after three days of feeding on 0 ("mock", n=234), 20 (n=192) and 50μg (n=99) per vial of RU486. **G**. Total numbers of ISCs and EBs in the pairs in the conditions described in E. Overall numbers of ISCs/EBs in these genotypes are 765/737 (wild type), 790/752 (*N$^{55e11/+}$*) and 804/1148 (*l(1)N^B*) (de Navascués et al., 2012). **H**. Overall numbers of ISC/EB in the conditions described in F. In E-H, triangles with colour gradient indicate

642 the relative levels of Notch signalling: wild-type (white), excessive (red) or
643 defective (blue).

644 **Figure 2**. Parameter space and dynamic behaviour of the model. **A**. Stable
645 solutions of the system classified according to their resulting signalling state.
646 Green stands for symmetric positive fates (EB-EB pairs), blue represents
647 symmetric negative fates (ISC-ISC pairs), and orange denotes asymmetric
648 fates (ISC-EB pairs). The threshold in Notch level for EB identification is taken
649 to be equal to 0.1 (see the text for more details). Dotted line, boundary of
650 stability for steady states with identical cells; these 'homogeneous' solutions
651 are stable above the line. **B-E**. Time evolution (in arbitrary units) of Notch and
652 Delta activity in pairs of cells interacting with parameters from the points
653 indicated as 1 to 4 in (A). Parameter values in point 1 correspond to those
654 used in Collier et al. (1996) (B), while parameter values in points 2-4 (C-E)
655 correspond to examples of other asymmetric pairs, and symmetric positive
656 and symmetric negative pairs.

657 **Figure 3**. Variability in contact area, and distribution of Notch and Delta at the
658 membrane. **A**. Confocal stacks projected in Z, showing variability in contact
659 length (as proxy for area). Scale bar: 20μm. **B**. (i, ii) Side views of the
660 intestinal epithelium, showing the apical-basal distribution of Notch and Arm.
661 Lumen is at the top and basal at the bottom. (iii-v) Top view of the intestinal
662 epithelium (iii) with ZY and XZ side views (iv, v) corresponding to the marked
663 lines in (iii). Lumen is at the top and right of the XZ and ZY views,
664 respectively. **C**. Top view of the intestinal epithelium, with ZY and XZ side
665 views corresponding to the marked lines in the top view panel. The top view
666 panel is a z-projection illustrating the membrane localisation of Delta, with side
667 views showing its apical-basal distribution. Lumen is at the top and right of the
668 XZ and ZY views, respectively. Scale bars in B, C are 10μm. **D-F**. Arm (D),
669 Delta (E) and Notch (F) levels along the perimeter of the cell planes (colour
670 lines) and mean (white). For each cell plane, position 0 corresponds to the
671 centre of the contacting membranes (defined as the position that intersects

672 the line connecting the cell centroids in that plane). Data in D and F are from
673 20 paired cells; data in E are from 43 cells.

674 **Figure 4**. The model can reproduce the observed cell fate profiles. Statistical
675 comparisons between data distributions in A-B, D-F were performed with the
676 Kolmogorov-Smirnov test. **A**. Swarm/box plots showing contact area values
677 segregated by fate profiles (11 ISC-ISC, 218 ISC-EB and 42 EB-EB pairs).
678 See main text. **B**. Swarm/box plots showing cell size values (measured as
679 projected areas) of ISCs and EBs. Projected areas correlate well with cell
680 volumes (Fig. S6A), which also shows a similar difference between ISCs and
681 EBs (Fig. S6B). **C**. Frequency of contact area values for nests of two
682 undifferentiated cells, irrespective of pair type. The red line marks the Smooth
683 Kernel Distribution (SKD) used to generate areas for the simulation. **D**.
684 Cumulative frequency of the contact area data for ISC-ISC and ISC-EB pairs.
685 **E**. Cumulative frequency of cell size (projected area) of ISCs and EBs. Blue
686 and light green lines correspond to the data depicted in B. Increasingly darker
687 green lines correspond to the cell size distributions of EBs which are smaller
688 than 1.0, 0.75 and 0.5 times the maximal ISC size, respectively. **F**. Cumulative
689 frequency of contact area of ISC-ISC (blue line) and ISC-EB (orange) pairs.
690 Increasingly darker orange lines correspond to the contact area distributions
691 of ISC-EB pairs with size limits of the EB of the pair is as in E. Data in B-F are
692 from a separate, larger dataset than that in A. **G**. Inset of the phase space
693 (corresponding to the white square in Fig. 2A), with shaded boxes indicating
694 the ranges of a and b values where the pair type frequencies from Fig. 1E
695 (upper panel) and Fig. 1F (lower panel) best fit the model. For each
696 experimental condition the height of the box is determined by the
697 neighbourhood of b values where $H \leq 0.02$; the values of a determining the
698 width of the box are obtained from Eqn. 7 using the best fitting value for c
699 (when b equals the value at the mid-height of the box) and the SKD depicted
700 in C to obtain experimentally supported values for A. Note the difference in
701 scale between the two axes, evident even with the log-log scale. **H**. Fate
702 outputs for the lateral inhibition model for different amounts of contact area.

703 The order of fate outcomes with increasing contact area follows the
704 experimental data in A.

705 **Table 1.** Cell-fate profiles as obtained experimentally ('data' column) and
706 theoretically ('model' column). The values of b are those at the mid-height of
707 the boxes in Fig. 4G corresponding to each of the genetic conditions in the
708 table. The values of c are those with lowest value of Kullback-Leibler entropy
709 H when b takes the value in the same row of this table.

dataset	condition	pair type	pair frequency		parameter value intervals		H
			data	model	b	c	
Figure 1E	$N^{ts1/+}$	ISC-ISC	4.7 %	5.1 %	0.26 ± 0.05	11	1.8×10^{-4}
		EB-EB	10.6 %	10.7 %			
		ISC-EB	84.7 %	84.2 %			
	$l(1)N^{B}/+$	ISC-ISC	0 %	0.7 %	0.15 ± 0.07	1.75	1.3×10^{-2}
		EB-EB	13.4 %	17.4 %			
		ISC-EB	86.6 %	81.9 %			
	$N^{55e11}/+$	ISC-ISC	12.2 %	11.7 %	0.20 ± 0.03	16	2.9×10^{-4}
		EB-EB	5.6 %	6.1 %			
		ISC-EB	82.2 %	82.2 %			
Figure 1F *da-GS, UAS-N^{RNAi}* (3 days with RU486)	mock	ISC-ISC	20.5 %	18.8 %	0.24 ± 0.03	23	1.5×10^{-3}
		EB-EB	22.7 %	24.6 %			
		ISC-EB	56.8 %	56.6 %			
	20μg	ISC-ISC	70.3 %	69.9 %	0.174 ± 0.004	49	3.9×10^{-4}
		EB-EB	3.7 %	4.2 %			
		ISC-EB	26.0 %	25.9 %			
	50μg	ISC-ISC	89.9 %	90.0 %	0.174 ± 0.004	64	1.6×10^{-2}
		EB-EB	1.0 %	3.4 %			
		ISC-EB	9.1 %	6.6 %			

710

711

References

Agrawal, S., Archer, C. and Schaffer, D. V. (2009). Computational Models of the Notch Network Elucidate Mechanisms of Context-dependent Signaling. *PLoS Comput Biol* **5**, e1000390–14.

Alcolea, M. P., Greulich, P., Wabik, A., Frede, J., Simons, B. D. and Jones, P. H. (2014). Differentiation imbalance in single oesophageal progenitor cells causes clonal immortalization and field change. *Nature Cell Biology* **16**, 615–622.

Arias, A. M. and Stewart, A. (2002). *Molecular Principles of Animal Development*. Oxford University Press, USA.

Artavanis-Tsakonas, S., Rand, M. D. and Lake, R. J. (1999). Notch signaling: cell fate control and signal integration in development. *science (New York, NY)* **284**, 770–776.

Baker, A.-M., Cereser, B., Melton, S., Fletcher, A. G., Rodriguez-Justo, M., Tadrous, P. J., Humphries, A., Elia, G., McDonald, S. A. C., Wright, N. A., et al. (2014). Quantification of crypt and stem cell evolution in the normal and neoplastic human colon. *CellReports* **8**, 940–947.

Bardin, A. J., Perdigoto, C. N., Southall, T. D., Brand, A. H. and Schweisguth, F. (2010). Transcriptional control of stem cell maintenance in the Drosophila intestine. *Development* **137**, 705–714.

Biteau, B., Hochmuth, C. E. and Jasper, H. (2008). JNK activity in somatic stem cells causes loss of tissue homeostasis in the aging Drosophila gut. *Cell Stem Cell* **3**, 442–455.

Boareto, M., Jolly, M. K., Lu, M., Onuchic, J. N., Clementi, C. and Ben-Jacob, E. (2015). Jagged–Delta asymmetry in Notch signaling can give rise to a Sender/Receiver hybrid phenotype. *Proceedings of the National Academy of Sciences* **112**, E402–E409.

Bray, S. and Furriols, M. (2001). Notch pathway: making sense of suppressor of hairless. *Curr Biol* **11**, R217–21.

Brennan, K., Tateson, R., Lewis, K. and Arias, A. M. (1997). A functional analysis of Notch mutations in Drosophila. *Genetics* **147**, 177–188.

Collier, J. R., Monk, N. A., Maini, P. K. and Lewis, J. H. (1996). Pattern formation by lateral inhibition with feedback: a mathematical model of delta-notch intercellular signalling. *J Theor Biol* **183**, 429–446.

de Back, W., Zhou, J. X. and Brusch, L. (2013). On the role of lateral stabilization during early patterning in the pancreas. *Journal of The Royal Society Interface* **10**, 20120766.

de Navascués, J., Perdigoto, C. N., Bian, Y., Schneider, M. H., Bardin, A. J., Martinez-Arias, A. and Simons, B. D. (2012). Drosophila midgut homeostasis involves neutral competition between symmetrically dividing intestinal stem cells. *EMBO J* **31**, 2473–2485.

Doupé, D. P., Alcolea, M. P., Roshan, A., Zhang, G., Klein, A. M., Simons, B. D. and Jones, P. H. (2012). A Single Progenitor Population Switches Behavior to Maintain and Repair Esophageal Epithelium. *science (New York, NY)* **337**, 1091–1093.

Dutta, D., Dobson, A. J., Houtz, P. L., Gläßer, C., Revah, J., Korzelius, J., Patel, P. H., Edgar, B. A. and Buchon, N. (2015). Regional Cell-Specific Transcriptome Mapping Reveals Regulatory Complexity in the Adult Drosophila Midgut. *CellReports* 1–14.

Ehebauer, M., Hayward, P. and Arias, A. M. (2006). Notch, a universal arbiter of cell fate decisions. *science (New York, NY)* **314**, 1414–1415.

Fang, H. Y., Martinez-Arias, A. and de Navascués, J. (2016). Autocrine and paracrine Wingless signalling in the Drosophila midgut by both continuous gradient and asynchronous bursts of wingless expression. *F1000Res* **5**, 317–14.

Formosa-Jordan, P., Ibanes, M., Ares, S. and Frade, J. M. (2012). Regulation of neuronal differentiation at the neurogenic wavefront. *Development* **139**, 2321–2329.

Friedmann, D. R. and Kovall, R. A. (2010). Thermodynamic and structural insights into CSL-DNA complexes. *Protein Science* **19**, 34–46.

Goulas, S., Conder, R. and Knoblich, J. A. (2012). The Par Complex and Integrins Direct Asymmetric Cell Division in Adult Intestinal Stem Cells. *Cell Stem Cell* **11**, 529–540.

Greenwald, I. (1998). LIN-12/Notch signaling: lessons from worms and flies. *Genes & Development* **12**, 1751–1762.

Guo, Z. and Ohlstein, B. (2015). Bidirectional Notch signaling regulates Drosophila intestinal stem cell multipotency. *science (New York, NY)* **350**, aab0988–aab0988.

Hsu, C.-P., Lee, P.-H., Chang, C.-W. and Lee, C.-T. (2006). Constructing quantitative models from qualitative mutant phenotypes: preferences in selecting sensory organ precursors. *Bioinformatics* **22**, 1375–1382.

Khait, I., Orsher, Y., Golan, O., Binshtok, U., Gordon-Bar, N., Amir- Zilberstein, L. and Sprinzak, D. (2015). Quantitative analysis of Delta-like-1 membrane dynamics elucidates the role of contact geometry on Notch signaling. *cell reports* **In Press**, 1–27.

Kidd, S., Lockett, T. J. and Young, M. W. (1983). The Notch locus of Drosophila melanogaster. *Cell* **34**, 421–433.

Kim, N.-G., Koh, E., Chen, X. and Gumbiner, B. M. (2011). E-cadherin mediates contact inhibition of proliferation through Hippo signaling-pathway components. *Proceedings of the National Academy of Sciences* **108**, 11930–11935.

Klein, A. M. and Simons, B. D. (2011). Universal patterns of stem cell fate in cycling adult tissues. *Development* **138**, 3103–3111.

Koch, U., Lehal, R. and Radtke, F. (2013). Stem cells living with a Notch. *Development* **140**, 689–704.

Krieger, T. and Simons, B. D. (2015). Dynamic stem cell heterogeneity. *Development* **142**, 1396–1406.

Kullback, S. and Leibler, R. A. (1951). On Information and Sufficiency. *Ann. Math. Statist.* 79–86.

LeVeque, R. J. (2007). Finite difference methods for ordinary and partial differential equations: steady-state and time-dependent problems (Vol. **98**). SIAM.

Lyman, D. and Young, M. W. (1993). Further evidence for function of the Drosophila Notch protein as a transmembrane receptor. *Proc Natl Acad Sci USA* **90**, 10395–10399.

Maeda, K., Takemura, M., Umemori, M. and Adachi-Yamada, T. (2008). E-cadherin prolongs the moment for interaction between intestinal stem cell and its progenitor cell to ensure Notch signaling in adult Drosophila midgut. *Genes Cells* **13**, 1219–1227.

Manders, E. M. M., Verbeek, F. J. and Aten, J. A. (1993). Measurement of co-localization of objects in dual-colour confocal images. *Journal of Microscopy* **169**, 375–382.

Micchelli, C. A. and Perrimon, N. (2006). Evidence that stem cells reside in the adult Drosophila midgut epithelium. *Nature* **439**, 475–479.

Miller, K. G., Field, C. M. and Alberts, B. M. (1989). Actin-binding proteins from Drosophila embryos: a complex network of interacting proteins detected by F-actin affinity chromatography. *The Journal of Cell Biology* **109**, 2963–2975.

Montagne, C. and González-Gaitán, M. (2014). Sara endosomes and the asymmetric division of intestinal stem cells. *Development* **141**, 2014–2023.

Muñoz-Descalzo, S., Tkocz, K., Balayo, T. and Arias, A. M. (2011). Modulation of the ligand-independent traffic of Notch by Axin and Apc contributes to the activation of Armadillo in Drosophila. *Development* **138**, 1501–1506.

Nagarkar-Jaiswal, S., Lee, P. T., Campbell, M. E. and Chen, K. (2015). A library of MiMICs allows tagging of genes and reversible, spatial and temporal knockdown of proteins in Drosophila. *eLife*.

Ohlstein, B. and Spradling, A. (2006). The adult Drosophila posterior midgut is maintained by pluripotent stem cells. *Nature* **439**, 470–474.

Ohlstein, B. and Spradling, A. (2007). Multipotent Drosophila intestinal stem cells specify daughter cell fates by differential notch signaling. *science (New York, NY)* **315**, 988–992.

Osterwalder, T., Yoon, K. S., White, B. H. and Keshishian, H. (2001). A conditional tissue-specific transgene expression system using inducible GAL4. *Proc Natl Acad Sci USA* **98**, 12596–12601.

Othmer, H. G. and Scriven, L. E. (1971). Instability and dynamic pattern in cellular networks. *J Theor Biol* **32**, 507–537.

Pei, Z. and Baker, N. E. (2008). Competition between Delta and the Abruptex domain of Notch. *BMC Dev Biol* **8**, 4.

Petrovic, J., Formosa-Jordan, P., Luna-Escalante, J. C., Abello, G., Ibanes, M., Neves, J. and Giraldez, F. (2014). Ligand-dependent Notch signaling strength orchestrates lateral induction and lateral inhibition in the developing inner ear. *Development* **141**, 2313–2324.

Plahte, E. (2001). Pattern formation in discrete cell lattices. *J Math Biol* **43**, 411–445.

Presente, A., Shaw, S., Nye, J. S. and Andres, A. J. (2002). Transgene-mediated RNA interference defines a novel role for notch in chemosensory startle behavior. *Genesis* **34**, 165–169.

Quiñones-Coello, A. T., Petrella, L. N., Ayers, K., Melillo, A., Mazzalupo, S., Hudson, A. M., Wang, S., Castiblanco, C., Buszczak, M., Hoskins, R. A., et al. (2007). Exploring strategies for protein trapping in Drosophila. *Genetics* **175**, 1089–1104.

Rouault, H. and Hakim, V. (2012). Different Cell Fates from Cell-Cell Interactions: Core Architectures of Two-Cell Bistable Networks. *Biophysj* **102**, 417–426.

Sanders, P. G. T., Muñoz-Descalzo, S., Balayo, T., Wirtz-Peitz, F., Hayward, P. and Arias, A. M. (2009). Ligand-independent traffic of Notch buffers activated Armadillo in Drosophila. *PLoS Biol* **7**, e1000169.

Schlegelmilch, K., Mohseni, M., Kirak, O., Pruszak, J., Rodriguez, J. R., Zhou, D., Kreger, B. T., Vasioukhin, V., Avruch, J., Brummelkamp, T. R., et al. (2011). Yap1 acts downstream of α-catenin to control epidermal proliferation. *Cell* **144**, 782–795.

Shaya, O. and Sprinzak, D. (2011). From Notch signaling to fine-grained patterning: Modeling meets experiments. *Curr. Opin. Genet. Dev.* 1–8.

Silvis, M. R., Kreger, B. T., Lien, W.-H., Klezovitch, O., Rudakova, G. M., Camargo, F. D., Lantz, D. M., Seykora, J. T. and Vasioukhin, V. (2011). α-catenin is a tumor suppressor that controls cell accumulation by regulating the localization and activity of the transcriptional coactivator Yap1. *Science Signaling* **4**, ra33–ra33.

Simons, B. D. and Clevers, H. (2011). Strategies for homeostatic stem cell self-renewal in adult tissues. *Cell* **145**, 851–862.

Simpson, P. (2001). Notch signalling in development: on equivalence groups and asymmetric developmental potential. *Curr. Opin. Genet. Dev.* **7**, 537–542.

Spradling, A. C., Stern, D., Beaton, A. and Rhem, E. J. (1999). The Berkeley Drosophila Genome Project gene disruption project: Single P-element insertions mutating 25% of vital Drosophila genes. *???*

Sprinzak, D., Lakhanpal, A., LeBon, L., Garcia-Ojalvo, J. and Elowitz, M. B.

(2011). Mutual Inactivation of Notch Receptors and Ligands Facilitates Developmental Patterning. *PLoS Comput Biol* **7**, e1002069.

Sprinzak, D., Lakhanpal, A., LeBon, L., Santat, L. A., Fontes, M. E., Anderson, G. A., Garcia-Ojalvo, J. and Elowitz, M. B. (2010). Cis-interactions between Notch and Delta generate mutually exclusive signalling states. *Nature* **465**, 86–90.

Tepass, U. and Hartenstein, V. (1994). The Development of Cellular Junctions in the Drosophila Embryo. *Developmental Biology* **161**, 563–596.

Tepass, U., Tanentzapf, G., Ward, R., & Fehon, R. (2001). Epithelial cell polarity and cell junctions in Drosophila. *Annual Review of Genetics* **35**, 747–784.

Tricoire, H., Battisti, V., Trannoy, S., Lasbleiz, C., Pret, A.-M. and Monnier, V. (2009). The steroid hormone receptor EcR finely modulates Drosophila lifespan during adulthood in a sex-specific manner. *Mech. Ageing Dev.* **130**, 547–552.

Vermeulen, L., Morrissey, E., van der Heijden, M., Nicholson, A. M., Sottoriva, A., Buczacki, S., Kemp, R., Tavaré, S. and Winton, D. J. (2013). Defining stem cell dynamics in models of intestinal tumor initiation. *science (New York, NY)* **342**, 995–998.

Zeng, X. and Hou, S. X. (2015). Enteroendocrine cells are generated from stem cells through a distinct progenitor in the adult Drosophila posterior midgut. *Development* **142**, 644–653.

Figure 1

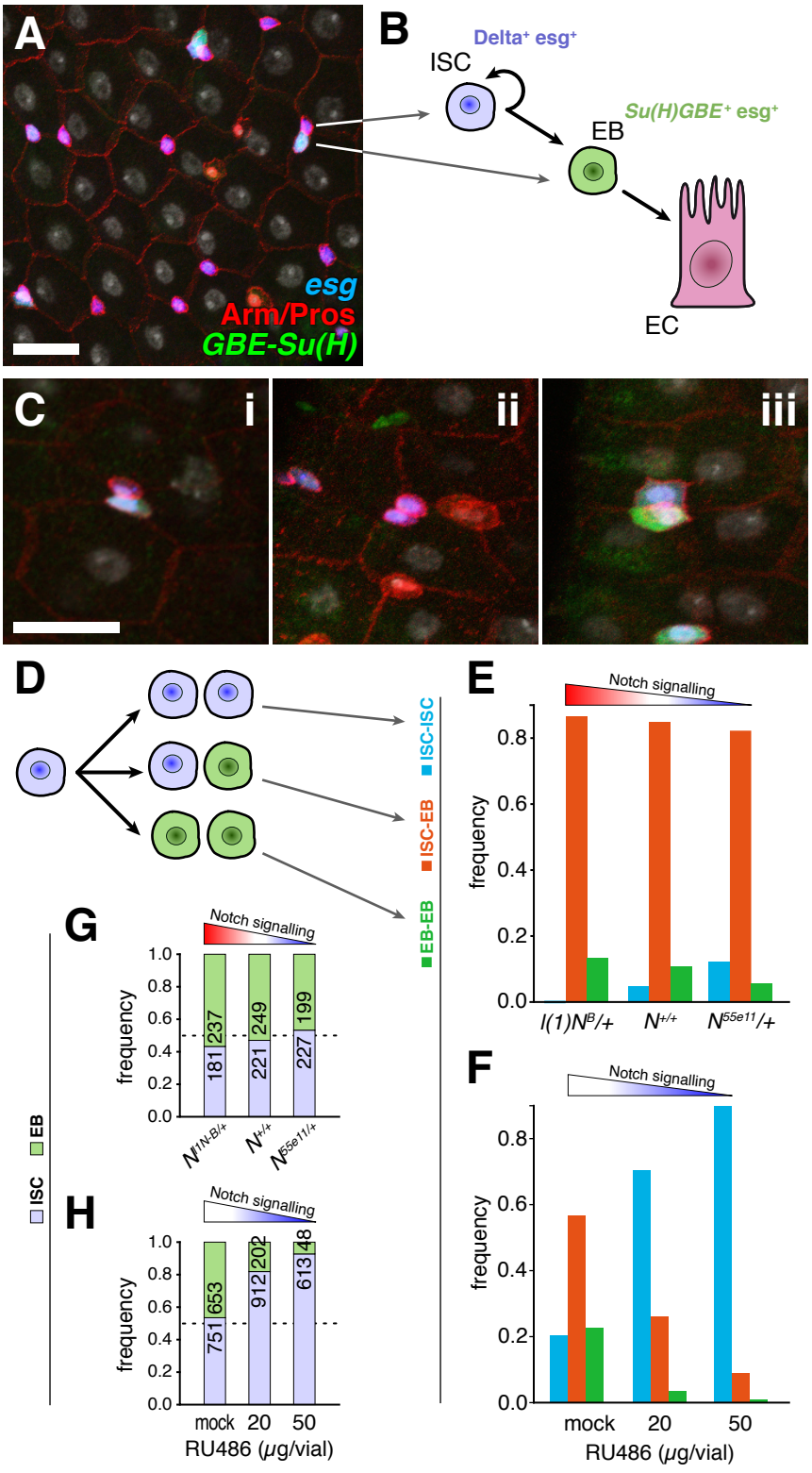
A
esg
Arm/Pros
GBE-Su(H)
B
Delta+ esg+
ISC
Su(H)GBE+ esg+
EB
EC
C
i
ii
iii
D
ISC-ISC
ISC-EB
EB-EB
E
Notch signalling
frequency
0.0
0.2
0.4
0.6
0.8
l(1)NB/+
N+/+
N55e11/+
F
Notch signalling
frequency
mock
20
50
RU486 (μg/vial)
G
Notch signalling
frequency
181
237
221
249
227
199
H
Notch signalling
frequency
751
653
912
202
613
48
mock
20
50
RU486 (μg/vial)
ISC
EB

Figure 2

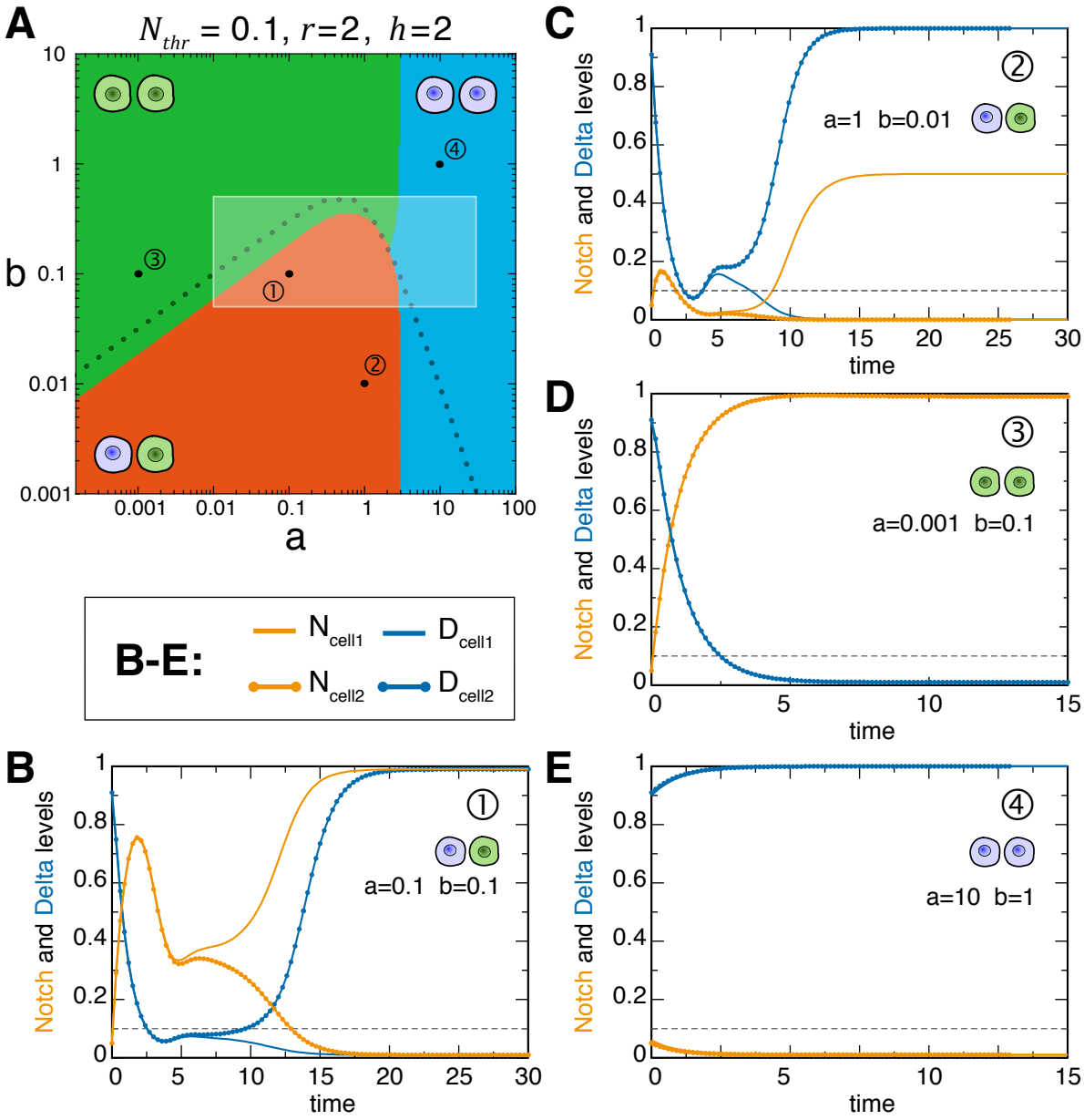
A
N_{thr} = 0.1, r=2, h=2
b
a
B-E:
N cell1
D cell1
N cell2
D cell2
B
C
D
E
Notch and Delta levels
time
a=0.1 b=0.1
a=1 b=0.01
a=0.001 b=0.1
a=10 b=1

Figure 3

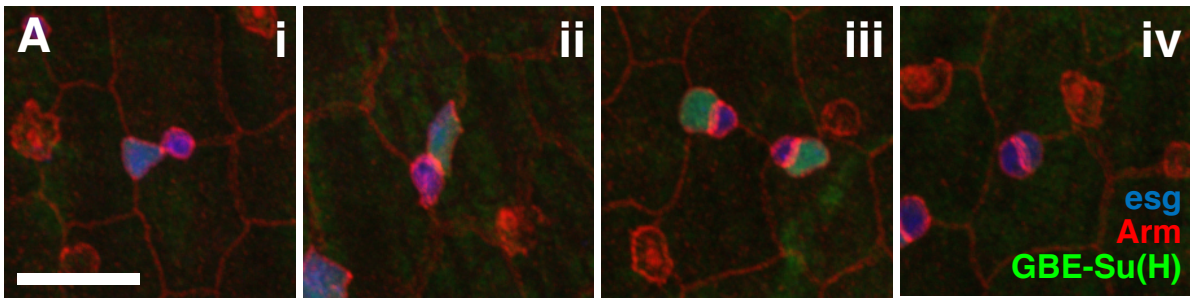
A
i
ii
iii
iv
esg
Arm
GBE-Su(H)

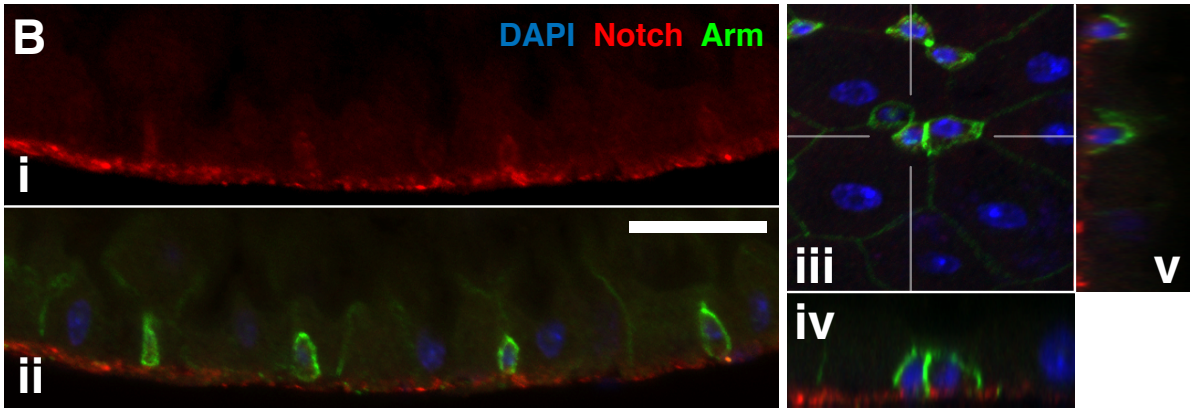
B
DAPI Notch Arm
i
ii
iii
iv
v

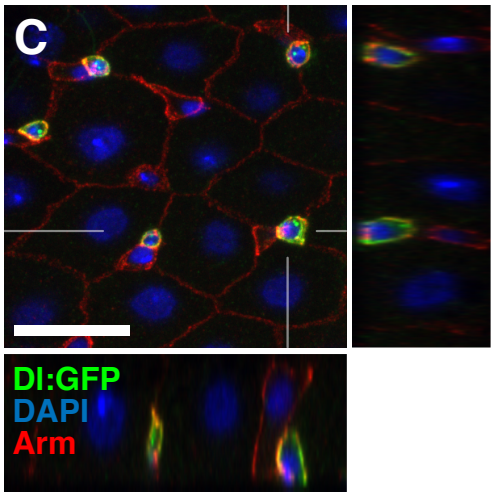
C
Dl:GFP
DAPI
Arm

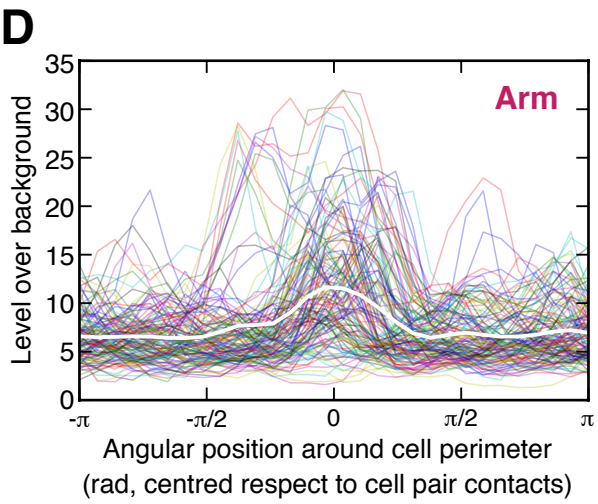
D
Arm
Level over background
35
30
25
20
15
10
5
0
-π
-π/2
0
π/2
π
Angular position around cell perimeter
(rad, centred respect to cell pair contacts)

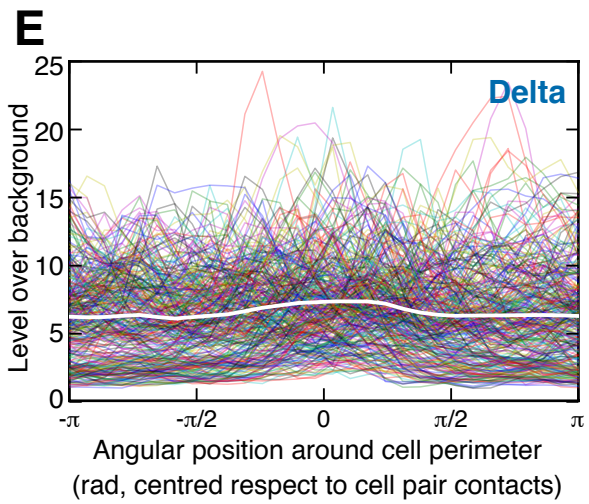
E
Delta
Level over background
25
20
15
10
5
0
-π
-π/2
0
π/2
π
Angular position around cell perimeter
(rad, centred respect to cell pair contacts)

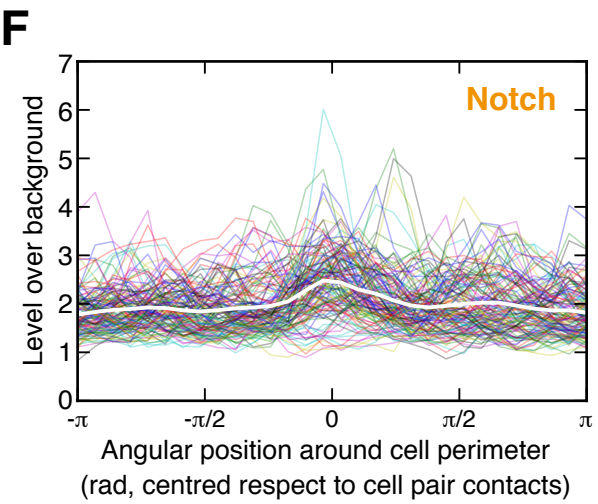
F
Notch
Level over background
7
6
5
4
3
2
1
0
-π
-π/2
0
π/2
π
Angular position around cell perimeter
(rad, centred respect to cell pair contacts)

Figure 4

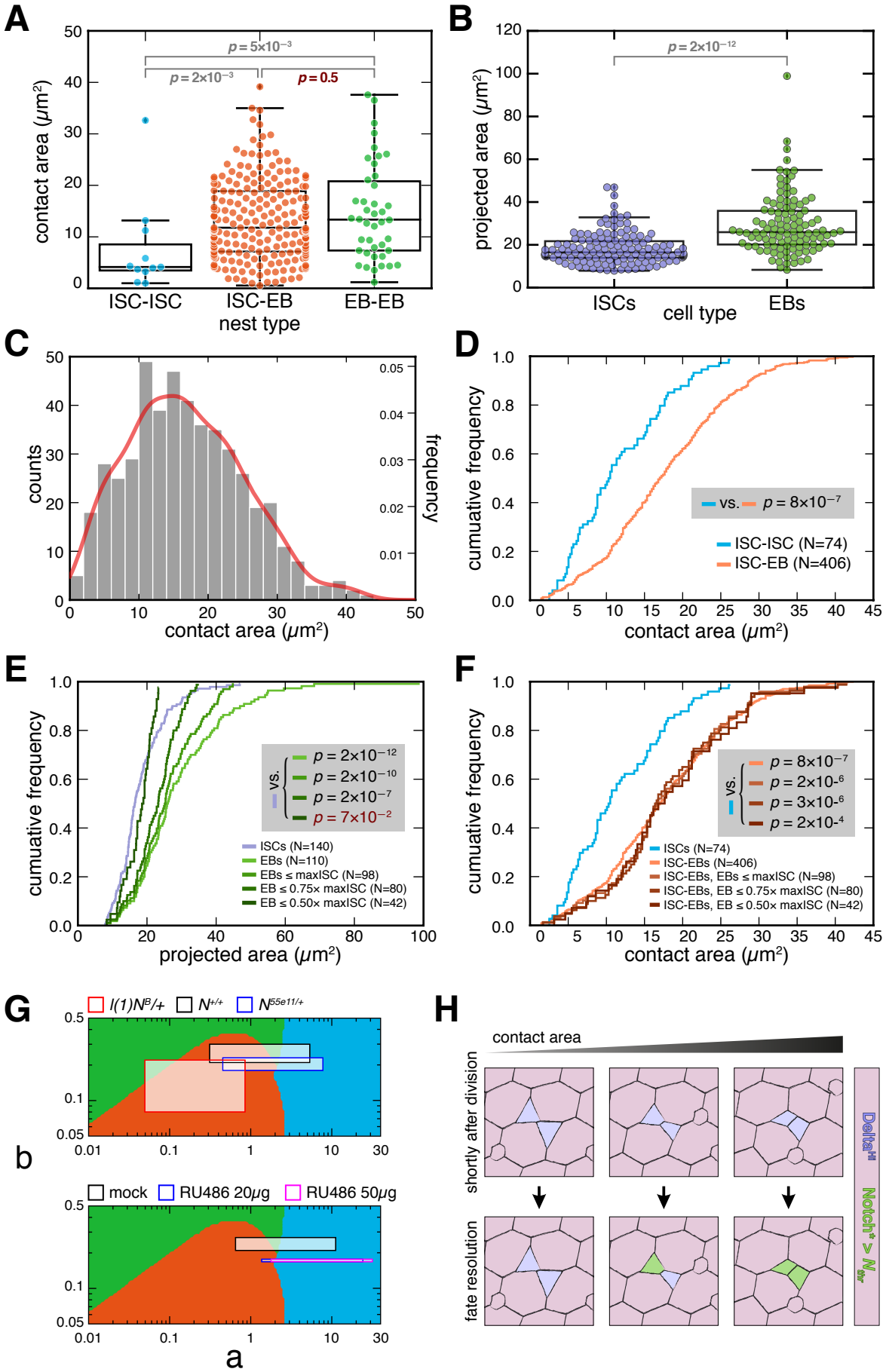
A
contact area (μm²)
p = 5×10⁻³
p = 2×10⁻³
p = 0.5
ISC-ISC
ISC-EB
EB-EB
nest type
B
projected area (μm²)
p = 2×10⁻¹²
ISCs
EBs
cell type
C
counts
frequency
contact area (μm²)
D
cumulative frequency
vs. p = 8×10⁻⁷
ISC-ISC (N=74)
ISC-EB (N=406)
contact area (μm²)
E
cumulative frequency
vs.
p = 2×10⁻¹²
p = 2×10⁻¹⁰
p = 2×10⁻⁷
p = 7×10⁻²
ISCs (N=140)
EBs (N=110)
EBs ≤ maxISC (N=98)
EB ≤ 0.75× maxISC (N=80)
EB ≤ 0.50× maxISC (N=42)
projected area (μm²)
F
cumulative frequency
vs.
p = 8×10⁻⁷
p = 2×10⁻⁶
p = 3×10⁻⁶
p = 2×10⁻⁴
ISCs (N=74)
ISC-EBs (N=406)
ISC-EBs, EBs ≤ maxISC (N=98)
ISC-EBs, EB ≤ 0.75× maxISC (N=80)
ISC-EBs, EB ≤ 0.50× maxISC (N=42)
contact area (μm²)
G
l(1)N^B/+
N^+/+
N^55e11/+
b
mock
RU486 20μg
RU486 50μg
a
H
contact area
shortly after division
fate resolution
Delta^hi
Notch^a > N_thr

Supplementary Figure S1. The model behaviour is robust to variations in N_{thr} and cooperativity strength. **A**. Fate profiles in parameter space as in Fig. 2A, for comparison. **B-E**. Phase space for N_{thr} equal to 0.8 (B), 0.3 (C), 0.01 (D), and 0.001 (E), respectively (with $r, h = 2$ in all cases). The dotted line marks the stability boundary for the 'homogeneous' solutions (pairs of identical cells), and serves as reference for comparison with (A). While in B (where $N_{thr} > 0.7$), the area of asymmetric fate is surrounded by symmetric negative resolution, in C-E the organisation of the phase space is very similar to A, with the transitions shifting along the stability boundary. **F-H**. Phase space when cooperativity is either increased (in the repression of Dl by activated N, with $h = 5$, in F; or in the activation of N by Dl, with $r = 5$, in G) or eliminated (with $r, h = 1$, in H). ($N_{thr} = 0.1$ in all cases). Phase space in F, G is qualitatively similar to A, but not in H, where the asymmetric pairs are lost.

Supplementary Figure S2. *Notch* knock-down using *da-GS* is EB and ISC-specific and can induce a phenotypic series. **A**. Confocal micrograph showing the expression pattern of the *da-GS* driver, shown with *UAS-Stinger*. The same panel is repeated three times: left, with all markers (Stinger, green; Delta/Prospero, red; *GBE-Su(H)-lacZ*, blue; DNA, grey), center, with Stinger and *GBE-Su(H)-lacZ* (purple) only, and right, with Stinger and Delta/Prospero (purple) only. Delta accumulates at the membrane and vesicles; Prospero is nuclear. Note expression is highly specific of ISCs (Delta$^+$) and EBs (*GBE-Su(H)-lacZ*$^+$), only occasionally showing expression in EEs (Pros$^+$; not shown). **B.** Cumulative frequency of nest size for *da-GS, UAS-N*^{RNAi} flies with different RU486 treatments, with N = {956, 782, 394, 457} for mock, 20, 50 and 500μg/vial, respectively. Note the similarity in distributions between mock, 20 and 50μg/vial (with only the latter having a barely significant p-value), which breaks down evidently with 500μg/vial. **C-F.** Confocal micrographs showing esg$^+$ cell nests after mock treatment (C) and *Notch* knock-down induced with 20 (D), 50 (E) and 500μg/vial (F), respectively. ISC-like tumours are starting to form only with the 500μg/vial treatment.

Supplementary Figure S3. Values of Notch and Delta at steady state across parameter space for $r = 2, h = 2$ (as in Figure 2A). Dotted line, boundary of stability for steady states with identical cells. The black dots mark the parameter values used in (Collier et al., 1996) (Figure 2B) and the asymmetric, symmetric positive and symmetric negative pairs from Figure 2C-E. **A, B.** Steady-state values of activated Notch in the two cells of a pair (one in each panel) respect to a, b. **C-D.** Steady-state values of Delta in the two cells of a pair (one in each panel) respect to a, b. Note that depending on the value of activated Notch, one can find symmetric negative or symmetric positive fate profiles below the boundary (region of heterogeneous solution), showing that the model allows for symmetric steady states where cells in a pair do not have identical amounts of Notch or Delta.

Supplementary Figure S4. Co-localisation between immunodetection of Delta and GFP using *Delta*$^{MI04868\text{-}GFSTF.1}$. **A.** Confocal micrograph illustrating the co-localisation of anti-Dl and anti-GFP in *Delta*$^{MI04868\text{-}GFSTF.1}$*/+* intestines. (Image shows the projection of several confocal planes). **B-C**. Co-localisation measurements between anti-Dl, anti-GFP (for *Delta*$^{MI04868\text{-}GFSTF.1}$), anti-Arm as a general membrane marker and Hoechst to label DNA, taken in 3D stacks for individual cells. N indicates the number of cells measured per experiment. Considering either Pearson correlation coefficient (B) or Manders co-localisation coefficient (C), the data show a high level of co-localisation between anti-Dl and anti-GFP, with very significantly higher coefficient values than between anti-GFP and Hoechst (which would give the baseline values for anti-correlation in this setting) as well as between anti-GFP and anti-Arm. The latter comparison indicates that the level of correlation between anti-Dl and anti-GFP cannot be from just coinciding randomly in the membrane and demonstrates that, at this level of spatial resolution, detection of *Delta*$^{MI04868\text{-}GFSTF.1}$ with anti-GFP is a very good indicator of the spatial distribution of Delta.

Supplementary Figure S5. Distribution of Arm, Notch and Delta at the membrane. **A-C.** Histograms of the normalised mean intensity per plane (left

hand panels) and the coefficient of variation (CV) per plane (right hand panels) for Arm (A), Notch (B) and Delta (C). The normalised mean intensity in plane *i* is defined as the ratio of the average of the plane and the average for the cell. Data correspond to 46 cells (single and paired) for Notch and Armadillo, and 66 cells (paired) for Delta. **D-F**. Distribution of Arm (D), Notch (E) and Dl (F) levels along the apical-basal cell axis (with height of the cell normalised to 1). Each cell contributes ten lines to the plot, corresponding to the intensity values along the vertical axis of non-overlapping, angular windows of 2π/10. Data displayed in D-E are from 20 paired esg+ cells and data in F are from 43 cells.

Supplementary Figure S6. Relationships between cell size, Arm levels and contact area, and statistical comparison between theoretical and experimental pair frequencies. Data in A-D are from the cell set from Figure 4B. **A**. Correlation between cell volume and projected cell area for EBs and ISCs, showing that projected area is a good predictor of total volume. **B**. Comparison of volume between ISCs and EBs. EBs are ~60% larger, with statistical significance. **C**. Correlation between contact area and projected cell area of the cells in the pair. The larger cells in each pair (usually an EB) is represented in dark blue and the smaller (usually an ISC) in light brown. **D**. Correlation between cell volume and projected cell area of the cells in the pair. Colour scheme is as in C. **E-F**. Arm levels along the perimeter of ISCs in either ISC-ISC (E) or ISC-EB (F) pairs, for all cells confocal planes (colour lines), with the mean value (white). For each cell plane, position 0 corresponds to the centre of the contacting membranes (defined as the position that intersects the line connecting the cell centroids in that plane). Data in E-F are from 20 ISC-EB and 23 ISC-ISC pairs. **G-H**. Kullback-Leibler relative entropy (*H*) between experimental and model distributions of *Notch* wild-type (G) or mock *Notch* knockdown (H) cell pair frequencies as a function of *b* and *c* (note the difference in scale between the two parameters). Values of area in the model are generated by the SKD depicted in Fig. 4C. Best fits (black dots) correspond to $b = 0.26$, $c = 11$ (G) and $b = 0.24$, $c = 23$ (H). Black

discontinuous lines mark isovalues every 0.05 H units. White discontinuous lines enclose the area for $H \leq 0.02$; the upper and lower limits of b in these areas define the height of the boxes in the parameter space indicated in Fig. 4G.

Supplementary Figure S1

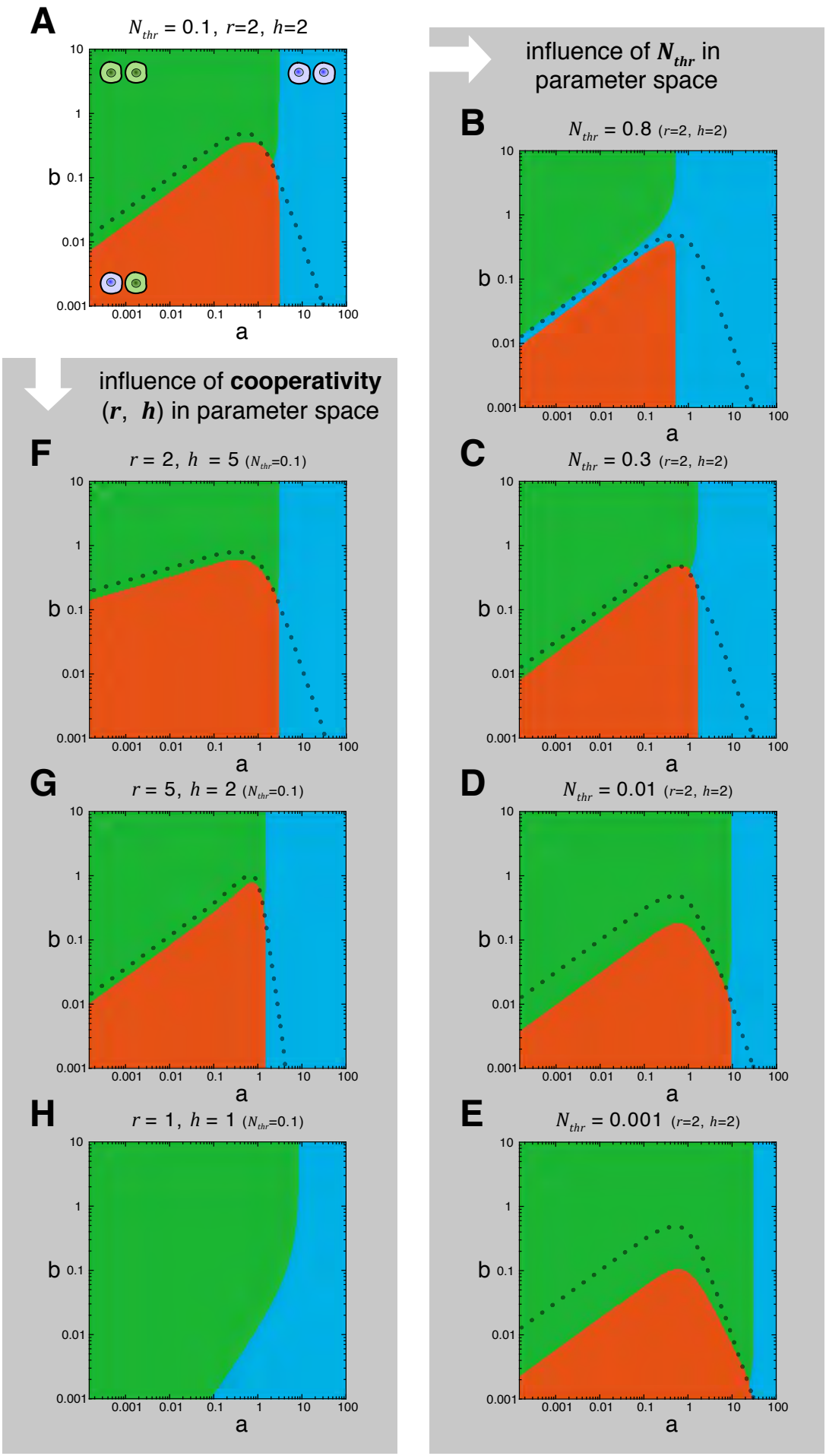

Supplementary Figure S2

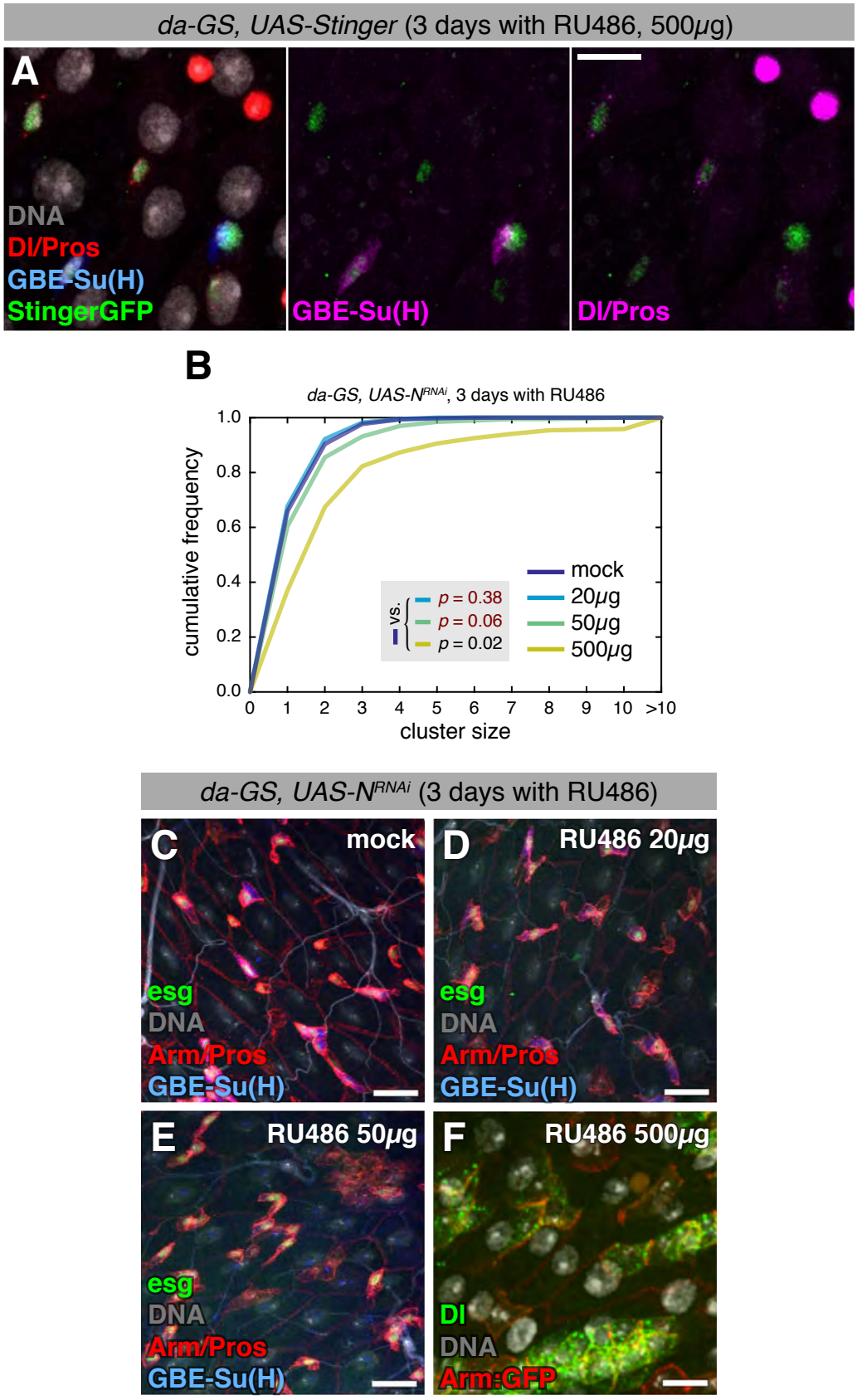

Supplementary Figure S3

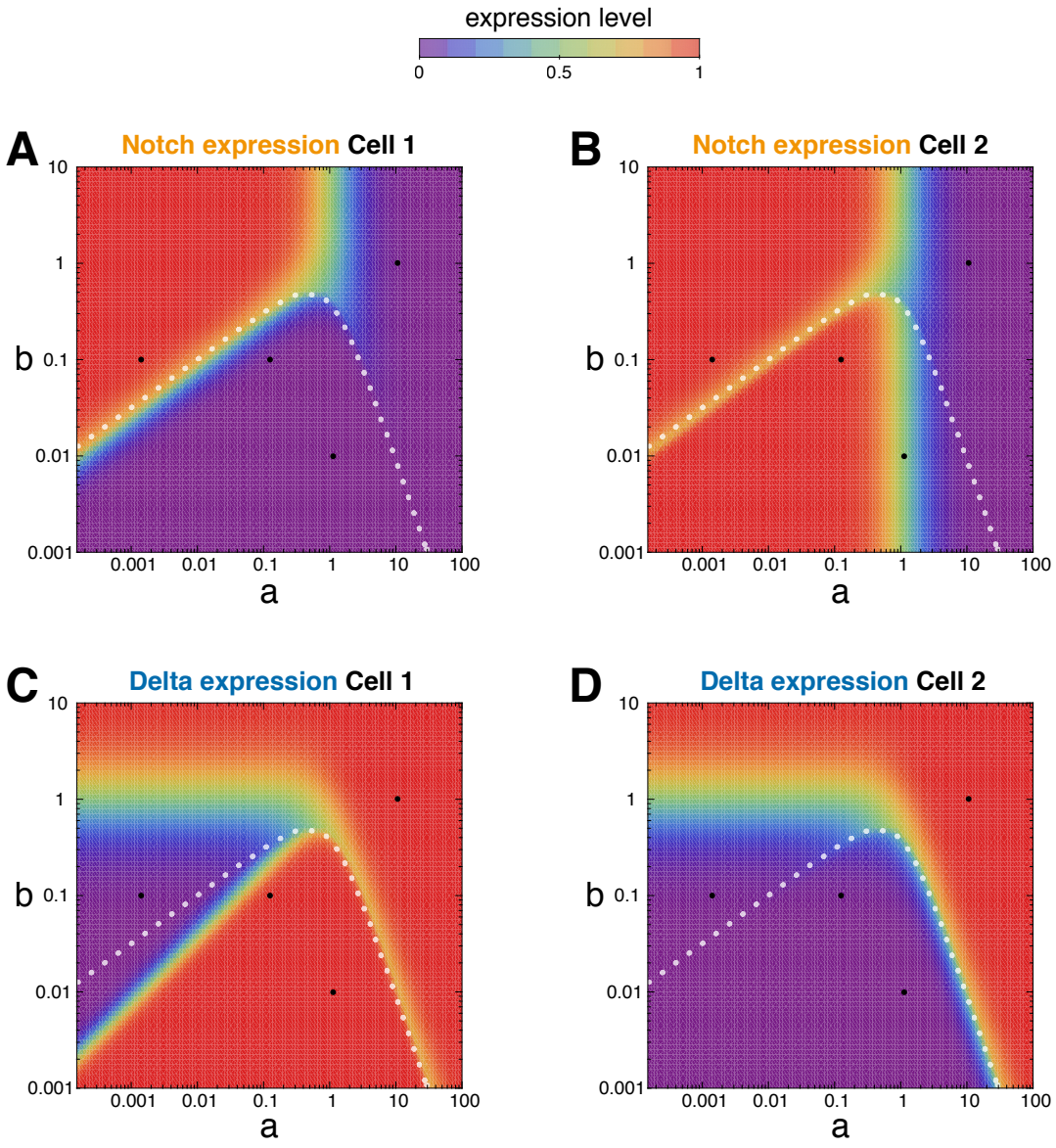

Supplementary Figure S4

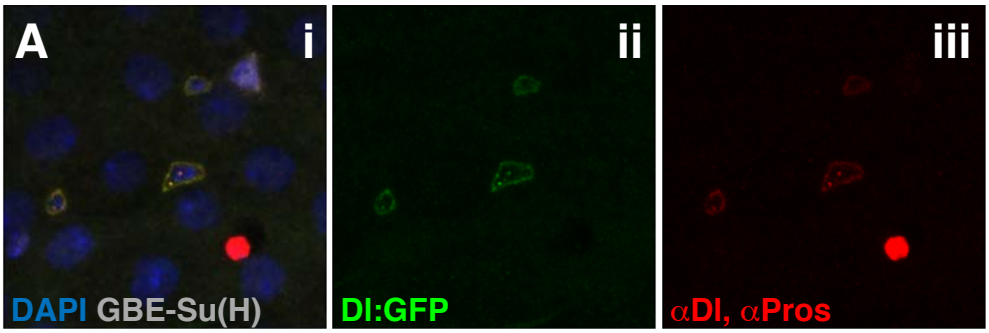

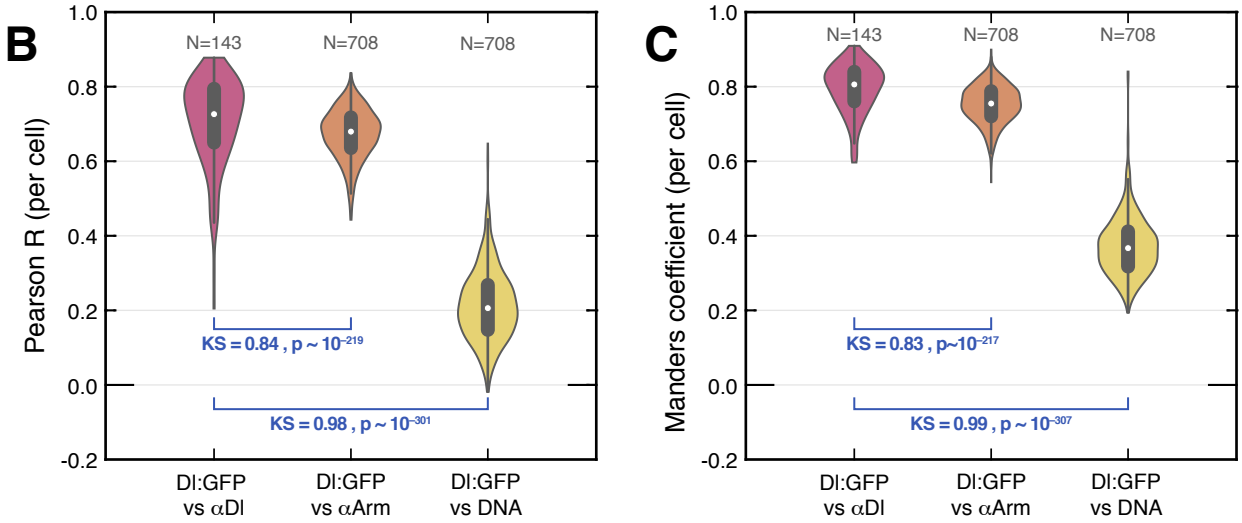

Supplementary Figure S5

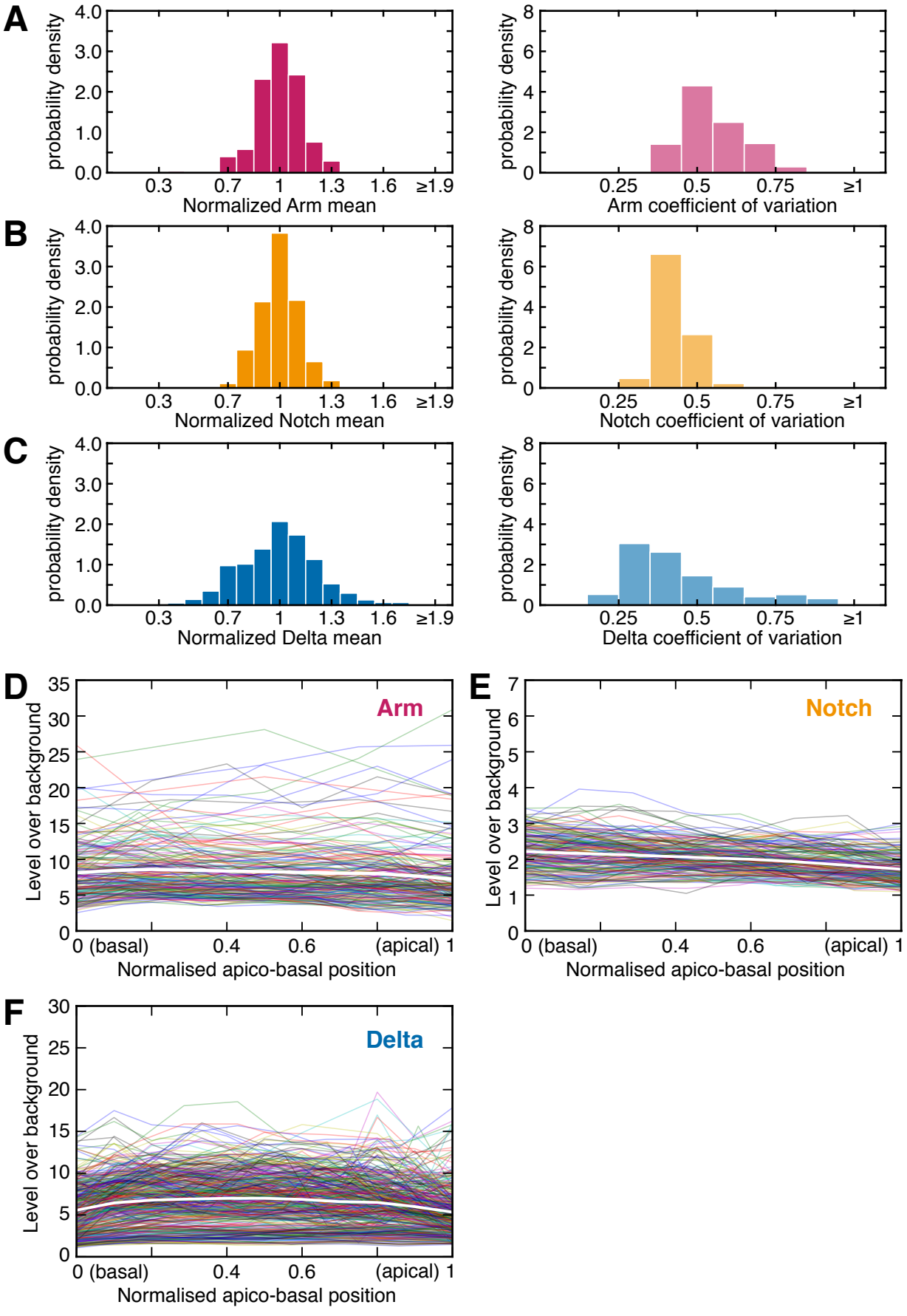

Supplementary Figure S6